Inorganic Chemistry
Article

Inorg. Chem. **2010**, *49*, 5079–5093 **5079**
DOI: 10.1021/ic100163g

Tetrahedral and Square Planar Ni[$(SPR_2)_2N]_2$ complexes, R = Ph & ^{i}Pr Revisited: Experimental and Theoretical Analysis of Interconversion Pathways, Structural Preferences, and Spin Delocalization

Dimitrios Maganas,[†,||] Alexios Grigoropoulos,[†] Sarah S. Staniland,[‡,#] Spyros D. Chatziefthimiou,[§] Andrew Harrison,[‡] Neil Robertson,[*,‡] Panayotis Kyritsis,[*,†] and Frank Neese[*,||]

[†]*Inorganic Chemistry Laboratory, Department of Chemistry, National and Kapodistrian University of Athens, GR−157 71 Athens, Greece,* [‡]*School of Chemistry and EaStChem, University of Edinburgh, West Mains Road, Edinburgh EH9 3JJ, United Kingdom,* [§]*EMBL−Hamburg c/o Deutsches Elektronen-Synchrotron, Hamburg, Germany, and* [||]*Institute of Theoretical and Physical Chemistry, Wegelerstrasse 12, D−53115 Bonn, Germany.* [#] *Present address: School of Physics and Astronomy, University of Leeds, Woodhouse Lane, Leeds LS2 9JT, United Kingdom.*

Received January 27, 2010

Sulfur-containing mono- or bidentate types of ligands, usually form square planar $Ni^{(II)}S_4$ complexes. However, it has already been established that the bidentate L^- dithioimidodiphosphinato ligands, $[R_2P(S)NP(S)R'_2]^-$, R, and R′ = aryl or alkyl, can afford both tetrahedral and square planar, NiS_4-containing, homoleptic $Ni^{R,R'}L_2$ complexes, owing to an apparent structural flexibility, which has not, so far, been probed. In this work, the literature tetrahedral $Ni[R_2P(S)NP(S)R_2]_2$ complexes, R = Ph ($Ni^{Ph,Ph}L_2$, $\mathbf{1}_{Td}$) and R = ^{i}Pr ($Ni^{iPr,iPr}L_2$, **2**) as well as the newly synthesized $Ni[^iPr_2P(S)NP(S)Ph_2]_2$ complex ($Ni^{iPr,Ph}L_2$, **3**), have been studied by UV−vis, IR, and ^{31}P NMR spectroscopy. Complex **3** was shown by X-ray crystallography to be square planar, and magnetic studies confirmed that it is diamagnetic in the solid state. However, it becomes paramagnetic in solution, as it shows a similar UV−vis spectrum to one of the tetrahedral $\mathbf{1}_{Td}$ and **2** complexes. The crystal structure of the potassium salt of the asymmetric ligand, $[^iPr_2P(S)NP(S)Ph_2]K$, has also been determined and compared to those of the protonated $^iPr_2P(S)NHP(S)Ph_2$ ligand and complex **3**. All three, $\mathbf{1}_{Td}$, **2**, and **3**, $Ni^{R,R'}L_2$ complexes show strong paramagnetic effects in their solution ^{31}P NMR spectra. The magnetic properties of paramagnetic complexes **1** and **2** in the solid state were investigated on oriented crystals, and their analysis afforded remarkably small values of the spin−orbit coupling constant (λ) and orbital reduction factor (k) parameters, implying significant delocalization of unpaired electronic density toward the ligands. The above experimental findings are combined with data from standard density functional theory and correlated multiconfiguration ab initio theoretical methods, in an effort to investigate the interplay between the square planar and tetrahedral geometries of the NiS_4 core, the mechanistic pathway for the spin-state interconversion, the degree of covalency of the Ni−S bonds, and the distribution of the spin density in this type of system. The analysis provides justification for the structural flexibility of such ligands, affording $Ni^{R,R'}L_2$ complexes with variable metallacycle conformation and NiS_4 core geometries. Of particular importance are the large zero-field splitting values estimated by both experimental and theoretical means, which have not, as yet, been verified by direct methods, such as electron paramagnetic resonance spectroscopy. The findings of our work confirm earlier observations on the feasibility of synthesizing either tetrahedral or square planar NiS_4 complexes containing the same type of ligands. They can also form the basis of investigating structure−properties relationships in other NiS_4-containing systems.

Introduction

A common feature in structural bioinorganic chemistry is the presence of sulfur-containing ligands in the active site of metalloproteins and metalloenzymes, most usually in the form of cysteine thiolate, S(Cys), or sulfide, S^{2-}.[1,2] Recent experimental and theoretical investigations have established that the electronic properties of these metalloproteins are highly dependent on the contribution of the sulfur valence orbitals to the "redox active" molecular orbitals of the active site, which is a measure of the covalency of the M−S bonds.[3,4] Crystallographic studies in the past few years have established that the active site of a range of nickel enzymes show

*To whom correspondence should be addressed. E-mail: Kyritsis@chem.uoa.gr (P.K.), neil.robertson@ed.ac.uk (N.R.), neese@thch.uni−bonn.de (F.N.).

(1) Holm, R. H.; Kennepohl, P.; Solomon, E. I. *Chem. Rev.* **1996**, *96*, 2239–2314.
(2) Rees, D. C.; Howard, J. B. *Science* **2003**, *300*, 929–931.
(3) Solomon, E. I.; Gorelsky, S. I.; Dey, A. *J. Comput. Chem.* **2006**, *27*, 1415–1428.
(4) Solomon, E. I. *Inorg. Chem.* **2006**, *45*, 8012–8025.

Published on Web 05/12/2010

remarkable variation in nickel coordination, and although the presence of Ni−S bonds in their active sites is rather prominent, they do not contain intact NiS_4 cores.[5] However, an artificial intact $[Ni^{(II)}S(Cys)_4]$ center has been generated by replacing $Fe^{(II)}$ by $Ni^{(II)}$ in the active site of rubredoxin. The Ni-substituted rubredoxin has been studied by X-ray crystallography[6] and spectroscopic methods,[7,8] with an aim of elucidating the structural and electronic properties of the metal site. In this case, the protein scaffold provides a rigid structural framework, imposing a tetrahedral (T_d) $Ni^{(II)}S_4$ metal core, rather similar to the structure of the $Fe^{(II)}S_4$ site in native rubredoxins.[6,8] On the other hand, extensive inorganic synthetic work has shown that $Ni^{(II)}S_4$-containing complexes usually exhibit square planar (SP) geometry, whereas the T_d geometry is rather rare.[9] It should be stressed that the interchange between SP and T_d geometries in NiS_4-containing complexes is not yet fully elucidated, despite promising theoretical efforts concerning tetra-coordinate transition-metal complexes.[10]

A search in the Cambridge Structural Database[11] reveals that only a handful out of over 800 complexes bearing the $Ni^{(II)}S_4$ core are not SP but instead display T_d geometry. The mononuclear T_d $Ni^{(II)}S_4$ complexes, that have been structurally characterized up to date, can be divided into two groups: (i) $Ni^{(II)}$ complexes bearing monodentate arylthiolato ligands of the $[Ni(SAr)_4]^{2-}$ general type,[12−18] and (ii) $Ni^{(II)}$ complexes bearing bidentate dithioimidodiphosphinato ligands, $Ni[R_2P(S)NP(S)R'_2]_2$, R, R′ = aryl or alkyl (denoted as $Ni^{R,R'}L_2$). The latter type of ligands are considered to be inorganic analogues of β-diketonates, and they readily form a wealth of $M^{(II)}L_2$ coordination compounds, containing six-membered chelating rings, that exhibit extensive delocalization of π-electronic density among the S−P−N−P−S fragment.[19−22] Furthermore, their wide S···S "bite" range (ca. 4 Å) allows them to satisfy the stereochemical requirements of different geometries.

The family of the $Ni^{R,R'}L_2$ complexes offers significant advantages in elucidating the electronic and stereochemical effects that favor the SP or T_d geometry in NiS_4 systems, given that, depending on the nature of the peripheral R groups, both geometries have been observed in such complexes under specific experimental conditions. More specifically, the T_d geometry is preferred when the ligand is symmetric, i.e., both P atoms bear the same peripheral groups (R = R′), as it can be deduced from the crystal structures of $Ni^{Me,Me}L_2$,[23] $Ni^{Ph,Ph}L_2$ (**1**$_{Td}$),[9,24] and $Ni^{iPr,iPr}L_2$ (**2**).[25] The structure of $Ni^{nBu,tBu}L_2$, in which each P atom is bonded to one ^{n}Bu and one ^{t}Bu group, has also revealed a T_d NiS_4 core.[26] It should be noted that, based on spectroscopic data, $Ni^{Ph,Ph}L_2$ was the first $Ni^{(II)}S_4$ complex reported to adopt a T_d geometry.[27] On the other hand, the complexes with asymmetric ligands (R = Ph and R′ = Me or ^{i}Pr) contain a SP NiS_4 core: the structure of $Ni^{Me,Ph}L_2$ has already been reported,[9] whereas the synthesis and structural characterization of $Ni^{iPr,Ph}L_2$ (**3**) is described herein.

The only exemption to the above general trend is $Ni^{Ph,Ph}L_2$, which has been also crystallized in a form containing a SP NiS_4 core (**1**$_{SP}$) and THF molecules.[28] To the best of our knowledge, $Ni^{Ph,Ph}L_2$ is the only NiS_4 complex that has been reported, up to date, to adopt, under different conditions, both a T_d and a SP geometry in the solid state. Such $Ni^{(II)}$ systems are expected to exhibit not only stereoisomerism but also spin isomerism, as the T_d complexes are typically paramagnetic ($S = 1$), whereas the SP ones are usually diamagnetic ($S = 0$),[29] although some exceptions have been documented by the identification of rare paramagnetic SP $Ni^{(II)}$ complexes.[30,31] In that respect, it is of interest to note that the ability of the dichalcogenated imidodiphosphinato ligands to form stereoisomers upon coordination to $Ni^{(II)}$ might be a general trend, since the corresponding $Ni[^iPr_2P(Se)NP(Se)^iPr_2]_2$ complex also affords both T_d and SP polymorphs.[32]

With the aim of advancing our previous investigations on analogous complexes of $Mn^{(II)}$ and $Co^{(II)}$,[33,34] we sought to explore the structural preferences and the electronic properties of $Ni^{R,R'}L_2$ complexes, both in the solid state and in solution, by employing magnetization, spectroscopic, and standard density functional theory (DFT) and correlated multiconfiguration ab initio theoretical methods. The questions addressed in this work are: (i) the interplay between SP and T_d geometries of the NiS_4 core, depending on the nature of the peripheral R groups as well as the mechanistic pathway

(5) Ragsdale, S. W. *J. Biol. Chem.* **2009**, *284*, 18571–18575.
(6) Maher, M.; Cross, M.; Wilce, M. C. J.; Guss, J. M.; Wedd, A. G. *Acta Crystallogr.* **2004**, *D60*, 298–303.
(7) Moura, I.; Teixeira, M.; Legall, J.; Moura, J. J. G. *J. Inorg. Biochem.* **1991**, *44*, 127–139.
(8) Goodfellow, B. J.; Duarte, I. C. N.; A. L. Macedo, A. L.; Volkman, B. F.; Nunes, S. G.; Moura, I.; Markley, J. L; Moura, J. J. G. *J. Biol. Inorg. Chem.* **2010**, *15*, 409–420.
(9) Rosler, R.; Silvestru, C.; EspinosaPerez, G.; Haiduc, I.; CeaOlivares, R. *Inorg. Chim. Acta* **1996**, *241*, 47–54.
(10) Cirera, J.; Alemany, P.; Alvarez, S. *Chem.—Eur. J.* **2004**, *10*, 190–207.
(11) Allen, F. H. *Acta Crystallogr.* **2002**, *B58*, 380–388.
(12) Yamamura, T.; Miyamae, H.; Katayama, Y.; Sasaki, Y. *Chem. Lett.* **1985**, 269–272.
(13) Rheingold, A. L.; Beall, K. S.; Riggs, P. J.; Groh, S. E. *Acta Crystallogr.* **1993**, *C49*, 542–543.
(14) Rosenfield, S. G.; Armstrong, W. H.; Mascharak, P. K. *Inorg. Chem.* **1986**, *25*, 3014–3018.
(15) Silver, A.; Koch, S. A.; Millar, M. *Inorg. Chim. Acta* **1993**, *205*, 9–14.
(16) Swenson, D.; Baenziger, N. C.; Coucouvanis, D. *J. Am. Chem. Soc.* **1978**, *100*, 1932–1934.
(17) Kockerling, M.; Henkel, G. *Z. Kristallogr.* **1994**, *209*, 186–187.
(18) Muller, A.; Henkel, G. *Z. Naturforsch.* **1995**, *50b*, 1464–1468.
(19) Woollins, J. D. *J. Chem. Soc., Dalton Trans.* **1996**, 2893–2901.
(20) Ly, T. Q.; Woollins, J. D. *Coord. Chem. Rev.* **1998**, *176*, 451–481.
(21) Silvestru, C.; Drake, J. E. *Coord. Chem. Rev.* **2001**, *223*, 117–216.
(22) Haiduc, I. Dichalcogenoimidodiphosphinato Ligands. In *Comprehensive Coordination Chemistry II: From Biology to Nanotechnology*; McCleverty, J. A., Meyer, T. J., Eds.; Elsevier: Amsterdam, 2003, Vol. *1*, pp 323−347.
(23) Churchil, M. R.; Cooke, J.; Fennessey, J. P.; Wormald, J. *Inorg. Chem.* **1971**, *10*, 1031–1035.
(24) Bhattacharyya, P.; Novosad, J.; Phillips, J.; Slawin, A. M. Z.; Williams, D. J.; Woollins, J. D. *J. Chem. Soc., Dalton Trans.* **1995**, 1607–1613.
(25) Cupertino, D.; Keyte, R.; Slawin, A. M. Z.; Williams, D. J.; Woollins, J. D. *Inorg. Chem.* **1996**, *35*, 2695–2697.
(26) Moore, P. Structure deposited in the Cambridge Structural Database as Personal Communication.
(27) Davison, A.; Switkes, E. S. *Inorg. Chem.* **1971**, *10*, 837–842.
(28) Simon−Manso, E.; Valderrama, M.; Boys, D. *Inorg. Chem.* **2001**, *40*, 3647–3649.
(29) Cirera, J.; Ruiz, E.; Alvarez, S. *Inorg. Chem.* **2008**, *47*, 2871–2889.
(30) Frommel, T.; Peters, W.; Wunderlich, H.; Kuchen, W. *Angew. Chem., Int. Ed.* **1993**, *32*, 907–909.
(31) Bridgeman, A. J. *Dalton Trans.* **2008**, 1989–1992.
(32) Levesanos, N.; Robertson, S. D.; Maganas, D.; Raptopoulou, C. P.; Terzis, A.; Kyritsis, P.; Chivers, T. *Inorg. Chem.* **2008**, *47*, 2949–2951.
(33) Maganas, D.; Staniland, S. S.; Grigoropoulos, A.; F. White, S. P.; Robertson, N.; Kyritsis, P.; Pneumatikakis, G. *Dalton Trans.* **2006**, 2301–2315.
(34) (a) Maganas, D.; Milikisyants, S.; Rijnbeek, J. M. A.; Sottini, S.; Levesanos, N.; Kyritsis, P.; Groenen, E. J. J. *Inorg. Chem.* **2010**, *49*, 595–605. (b) Sottini, S.; Mathies, G.; Gast, P.; Maganas, D.; Kyritsis, P.; Groenen, E. J. J. *Phys. Chem. Chem. Phys.* **2009**, *11*, 6727–6732.

for the spin-state interconversion, (ii) the degree of covalency of the Ni−S bonds, depending on the NiS_4 geometry, and (iii) the distribution of the spin density in the paramagnetic T_d complexes.

Experimental Section

Materials and Methods. All experiments were carried out under an atmosphere of argon using Schlenk techniques. The glassware was dried in the oven at approximately 110 °C and baked out in vacuo prior to use. The solvents were dried by standard methods (methanol and dichloromethane over CaH_2, *n*-hexane over sodium wire) and distilled under argon. The solvents were deoxygenated by at least three pump and purge cycles immediately prior to use. All chemical reagents were purchased from Aldrich. The LH ligands, $R_2P(S)NHP(S)R'_2$ (denoted as $^{R,R'}$LH), R=R′=Ph,[35] R=R′=^{i}Pr,[25] R=Ph, and R′=^{i}Pr[36] and their corresponding LK salts (denoted as $^{R,R'}$LK) as well as the complexes $\mathbf{1}_{Td}$,[9,24] $\mathbf{1}_{SP}$,[28] and **2**[25] were prepared according to published procedures.

UV−vis, IR, and NMR Spectroscopy. Electronic spectra were recorded in a Carry 300 Varian spectrophotometer. IR spectra were run in the range of 4000−200 cm^{-1} on a Perkin-Elmer 883 IR spectrophotometer, as KBR pellets. ^{1}H and ^{31}P−{^{1}H} spectra were recorded in a Varian Unity Plus 300 MHz instrument. The ^{1}H and ^{31}P−{^{1}H} chemical shifts are relative to $SiMe_4$ and to 85% H_3PO_4, respectively.

Magnetic Susceptibility Studies. Magnetic susceptibility measurements were carried out between 2 and 300 K, using a Quantum design MPMS2 SQUID magnetometer with MPMS MultiVu Application software to process the data. The magnetic field employed was 0.1 T. The program used for the simulation of magnetic data is presented in the Supporting Information.

X-ray Crystallography. Ligand ^{iPr,Ph}LK. : Low-temperature X-ray data were collected at the synchrotron radiation light source at EMBL−Hamburg, Deutsches Elektronen-Synchrotron (DESY), beamline X13, by the oscillation method using a CCD detector of 165 mm radius. A single crystal, covered with a drop of oil, was mounted on a small loop of hair fiber and was instantly frozen at 100 K. The programs DENZO and SCALEPACK[37] were used for data processing and scaling of data, respectively. The structure was solved by direct methods and refined by full-matrix least-squares based on F^2, using the program SHELXL97.[38] Hydrogen (H) atoms have been placed in idealized positions and refined by the riding model (U_H = 1.30 U_C).

Complex 3. : X-ray diffraction intensities were collected with Mo Kα radiation on a Bruker Smart APEX CCD diffractometer equipped with an Oxford Cryosystems low−temperature device operating at 150 K. Absorption corrections were carried out with the multiscan procedure SADABS. The structure was solved by direct methods (SHELXS97) and refined by full-matrix least-squares against $|F|^2$ using all data (SHELXL97). H atoms were placed in calculated positions and allowed to ride on their parent atoms. All non-H atoms were modeled with anisotropic displacement parameters.

The structural and refinement parameters for the ^{iPr,Ph}LK ligand and complex **3** are given in the Supporting Information, Table S1.

Computational Details. All electronic structure calculations reported in this paper were performed with the ORCA program.[39] For the DFT and the ab initio multiconfigurational self-consistent field theory (MCSCF) calculations, truncated models denoted as $Ni^{H,H}L_2$ in different spin states and conformations, as defined in the respective sections, were chosen, such as to keep the computational effort acceptable. For the DFT calculations, the BP86[40,41] and B3LYP[40,42,43] functionals were used for the calculation of geometries/frequencies and spectroscopic properties, respectively, together with a basis set of polarized triple-ζ (TZVP) quality. In order to compute the d−d transitions of $Ni^{(II)}$ complexes, the minimal active space should include the five 3d-based molecular orbitals involved in nonbonding or σ M−S antibonding interactions as well as the corresponding σ M−S bonding molecular orbitals. This leads to an active space with 12 electrons in 7 orbitals (CAS (12,7)). We have included all 10 roots for the triplet states (arising from the ^{3}F and ^{3}P terms of Ni^{2+}) and 5 singlet roots (arising from the ^{1}D term of Ni^{2+}). MR-difference dedicated CI calculations, with two degrees of freedom (DDCI2)[44] were performed on top of the state-averaged-complete active space self-consistent field (SA-CASSCF) reference wave function, in order to recover the major part of the differential dynamic correlation between the ground and excited states. As it was commented upon previously,[45] we have used individual selection in order to decrease the computation time. The size of the first-order interacting space was reduced with a threshold $T_{sel} = 10^{-6}$ Eh. A further approximation involves reduction of the reference space through rejection of all initial references that contribute less than a second threshold ($T_{pre} = 10^{-5}$) to the zeroth-order states. The minimum-energy crossing point (MECP) of the DFT $S = 0$ and 1 surfaces was identified via MECP optimizations, as implemented in the ORCA program.

Synthesis of K[^{i}Pr$_2$P(S)NP(S)Ph$_2$] (^{iPr,Ph}LK). In a Schlenk-type flask charged with 5 g (12.1 mmol) of ^{iPr,Ph}LH, 20 mL of MeOH are added under stirring. To the resulting suspension, 1.8 g of ^{t}BuOK are added at once. The white mixture is left stirring for 2 h. At this point, the white solid is filtered and washed with 3 × 10 mL of cold MeOH to yield 5.1 g (11.2 mmol) of ^{iPr,Ph}LK (93%). White needle-shaped crystals were obtained by slow evaporation of a chloroform solution of ^{iPr,Ph}LK. IR (cm^{-1}): ν(Ph_2P−S) 586s, ν(^{i}Pr_2P−S) 519s, ν(PNP) 1205br; ^{31}P NMR (121.75 MHz, $CDCl_3$, 303 K): δ_P (ppm) = 36.8 [s, Ph_2P], 72.4 [s, ^{i}Pr_2P].

Synthesis of Ni[^{i}Pr$_2$P(S)NP(S)Ph$_2$]$_2$ (3). In a Schlenk-type flask, 0.21 g (0.5 mmol) of ^{iPr,Ph}KL were dissolved into 20 mL of CH_3OH. The mixture was stirred at room temperature for 30 min, until complete dissolution was reached and, subsequently, 0.059 g (0.25 mmol) of $NiCl_2 \cdot 6H_2O$ were added. The solution turned gradually to dark green. After 2 h of stirring at room temperature, a green solid precipitated that was filtered off and washed with cold MeOH to yield 159.7 mg of **3** (78%). Dark-green needle-like crystals, suitable for X-ray diffraction studies, were grown by slow diffusion of *n*-hexane into a CH_2Cl_2 solution of **3** at 250 K. IR (cm^{-1}): ν(Ph_2P−S) 573s, ν(*i*Pr_2P−S) 527s, ν(PNP) 1231br; ^{1}H NMR (300 MHz, $CDCl_3$, 303 K): δ_H (ppm) = 7.8 [s, 4H, CH], 6.5 [br, 8H, *m*-C_6H_5], 6.03 [d, 4H, ^5J(PH) = 58.18 Hz, *p*-C_6H_5], 7.77 [d, 12H, ^3J(PH) = 123.49 Hz, CH_3], 8.41 [d, 8H, ^3J(PH) = 141.25 Hz, *o*-C_6H_5], 9.45 [s(br), 12H, CH_3]; ^{31}P NMR (121.75 MHz, $CDCl_3$, 303 K): δ_P (ppm) = −512.4 [s(br), Ph_2P], −555. [s(br), ^{i}Pr_2P].

(35) Wang, F. T.; Najdzionek, J.; Neneker, K. L.; Wasserman, H.; Braitsch, D. M. *Synth. React. Inorg. Met.−Org. Chem.* **1978**, *8*, 119–125.
(36) Birdsall, D. J.; Slawin, A. M. Z.; Woollins, J. D. *Polyhedron* **2001**, *20*, 125–134.
(37) Otwinowski, Z.; Minor, W. *Methods in Enzymology, Macromolecular Crystallography, Part A*; edited by Carter, C. W., Jr, Sweet, R. M., Eds.; Academic Press: New York, 1997; Vol. *276*, pp 307−326.
(38) Sheldrick, G. M. *SHELX97*, University of Göttingen: Göttingen, Germany, **1997**.
(39) Neese, F. *ORCA*, version 2.6.35; University of Bonn: Bonn, Germany, **2008**.
(40) Becke, A. D. *Phys. Rev. A: At., Mol., Opt. Phys.* **1988**, *38*, 3098–3100.
(41) Perdew, J. P. *Phys. Rev. B: Solid State* **1986**, *33*, 8822–8824.
(42) Becke, A. D. *J. Chem. Phys.* **1993**, *98*, 5648–5652.
(43) Lee, C.; Yang, W.; Parr, R. G. *Phys. Rev. B: Solid State* **1988**, *37*, 785–789.
(44) Miralles, J.; Castell, O.; Caballol, R.; Malrieu, J. P. *Chem. Phys.* **1993**, *172*, 33–43.
(45) Neese, F. *J. Chem. Phys.* **2003**, *119*, 9428–9443.

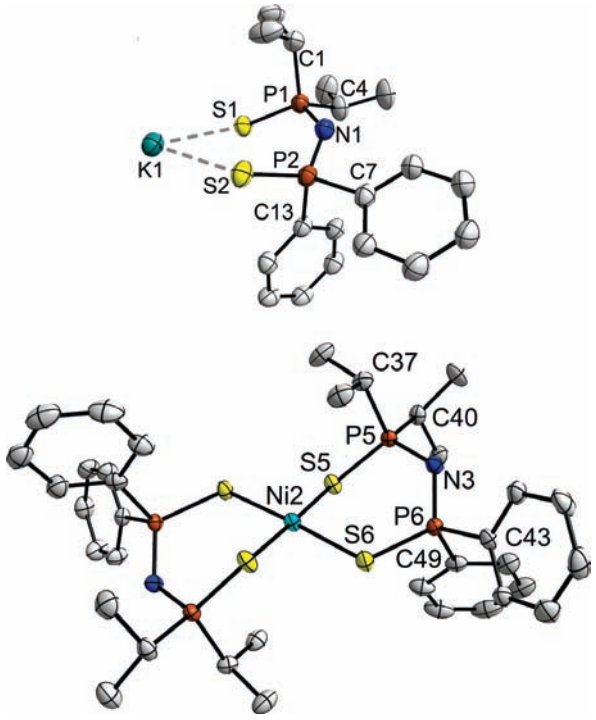

Figure 1. Thermal ellipsoid plot (50% probability) of the X-ray structure of the ^{iPr,Ph}LK ligand and the centrosymmetric complex **3b**.

Results and Discussion

Molecular Structures. The direct comparison between the protonated and anionic forms of the dithioimidodiphosphinato ligands was up to now possible only for the symmetric phenyl analogue, ^{Ph,Ph}LH, given that the crystal structure of both protonated[46,47] and deprotonated ^{Ph,Ph}LK[48] forms has been resolved. Herein, we report the first crystal structure of a deprotonated asymmetric ligand that belongs to the same family. ^{iPr,Ph}LK crystallizes in the space group $P2_1/c$. The ORTEP plot of ^{iPr,Ph}LK is shown in Figure 1, whereas selected bond lengths and angles are presented in the Supporting Information, Table S2. The P−N bonds are lengthened, the P−S bonds are shortened, and the P−N−P angle is slightly increased compared to the respective protonated ^{iPr,Ph}LH form.[36] This is a well documented trend,[21] originating from the enhanced delocalization among the S−P−N−P−S fragment and the ensuing higher sp^2 character of the nitrogen atom, upon deprotonation.[33]

The conformation of the M−S−P−N−P−S metallacycles is governed by the P−N−P−S torsion angles that define the orientation of the P−S bonds relatively to the P−N−P plane. In the crystal structure of ^{iPr,Ph}LK, the Ph_2P−S bond is rotated out of the PNP plane (P−N−P−S/Ph = 64.7°), whereas the $^{i}Pr_2$P−S bond lies in the P−N−P plane (P−N−P−S/^{i}Pr = 3°). Therefore, the K−S−P−N−P−S ring exhibits a distorted *boat* conformation, with P/Ph and S/^{i}Pr occupying the apexes. The fact that the $^{i}Pr_2$P−S bond is almost coplanar with the P−N−P backbone promotes the delocalization of π-electron density and thus its partial dissipation from the P atom bearing the electron-donating ^{i}Pr groups toward the P atom bearing the electron-withdrawing Ph groups. This electron density flow from "the alkyl towards the phenyl side" is demonstrated by the different P−N bond lengths and is also verified via ^{31}P NMR spectroscopy (vide infra).

On the contrary, the six-membered K−S−P−N−P−S ring of the symmetric ^{Ph,Ph}LK ligand adopts a perfect *twisted boat* conformation, where both the P−N−P−S torsion angles are equal (39.0°) and the Ph_2P−S bonds are orientated beneath and above the P−N−P plane, respectively. The overall symmetry of ^{Ph,Ph}LK is C_2, with the main axis defined by the K and N atoms and bisecting both S−K−S and P−N−P angles.[48] Therefore, the different electron-donating properties of the peripheral groups in ^{iPr,Ph}LK distorts the overall symmetry and gives rise to the boat conformation. It should be pointed out that the conformation of the metallacycle is not influenced by intermolecular interactions, since both ^{iPr,Ph}LK and ^{Ph,Ph}LK exhibit the same polymeric structure.

Complex **3** crystallizes in the space group *P*-1 as two crystallographically independent molecules **3a** and **3b**, selected bond lengths and angles of which are listed in the Supporting Information, Table S2. The only profound structural difference between **3a** and **3b** is the relative position of the methyl groups, i.e., the rotation around the P−C bonds. The presence of two H atoms near the vacant axial positions in **3b**—their distance from the central Ni atom being only 2.607 Å—possibly stabilizes the SP geometry. On the contrary, this close-contact interaction is absent (Ni···H = 2.722 Å) in the crystal structure of **3a** that exhibits a small tetrahedral distortion. Regardless of whether this hypothesis is correct or not, the tetrahedral distortion of **3a** indicates that the stabilization of the SP geometry for this family of NiS_4 complexes is marginal.

The ORTEP plot of the crystal structure of **3b** is shown in Figure 1. Complex **3b** is centrosymmetric, while complex **3a** deviates from C_i symmetry, since both trans S−Ni−S angles are less than 180°. The centrosymmetric structure contains a planar NiS_4 core (sum of S−Ni−S bond angles 360°), and the two asymmetric $^{iPr,Ph}L^-$ ligands are coordinated in a trans arrangement to each other. The Ni−S/Ph bonds (see Supporting Information, Table S2) are slightly longer (2.236 Å) than the Ni−S/^{i}Pr bonds (2.223 Å). Both bond lengths lie at the upper extreme of the range observed in SP NiS_4 complexes (2.11−2.25 Å)[9,11,49] and are significantly shorter than the Ni−S bond lengths in T_d $Ni^{R,R'}L_2$ analogues (2.28−2.30 Å).[11,23−26] The comparison between the two stereoisomers of the analogous Ni[$^{i}Pr_2$P(Se)NP(Se)$^{i}Pr_2$]$_2$ complex supports the latter observation, since the Ni−Se bond lengths were found shorter (2.354 Å) for the SP than the T_d isomer (2.400 Å).[32]

As it was discussed above, the extensive delocalization of π-electronic density due to deprotonation and coordination of the ligand results in the lengthening of the P−S bonds, the shortening of the P−N bonds, and the opening of the P−N−P angle, as compared to the free protonated

(46) Noth, H. *Z. Naturforsch.* **1982**, *37b*, 1491–1498.
(47) Husebye, S.; Maartmannmoe, K. *Acta Chem. Scand.* **1983**, *A37*, 439–441.
(48) Slawin, A. M. Z.; Ward, J.; Williams, D. J.; Woollins, J. D. *J. Chem. Soc. Chem. Commun.* **1994**, 421–422.
(49) Colpas, G. J.; Kumar, M.; Day, R. O.; Maroney, M. J. *Inorg. Chem.* **1990**, *29*, 4779–4788.

form. The comparison of the crystal structures of ^{iPr,Ph}LH,[36] ^{iPr,Ph}LK, and complex **3** can separate out the geometric changes caused by either the deprotonation of the ligand or its coordination to the $Ni^{(II)}$ center. As it can be deduced from the selected bond lengths and angles presented in the Supporting Information, Table S2, the P−S bonds are further lengthened upon coordination, while the P−N bonds remain practically unaffected.

Moreover, in complex **3**, the boat conformation of the Ni−S−P−N−P−S metallacycle is retained, with the P/Ph and S/^{i}Pr atoms lying at the apexes. The $^{i}Pr_2P$−S bonds are located in the P−N−P plane (torsion angle P−N−P−S/^{i}Pr = 0°), whereas the Ph_2P−S bonds are rotated out of it by 49°. The smaller torsion angle, compared to ^{iPr,Ph}LK, is a straightforward effect of the shorter covalent Ni−S bonds compared to the longer ionic K−S bonds. Therefore, the S···S bite is decreased from 4.15 Å in ^{iPr,Ph}LK to 3.37 Å in **3b**, resulting in an increased repulsive interaction between the S atoms and a greater degree of ring strain among the ligands. This is compensated, to a certain extent, by the relaxation of the endocyclic S−Ni−S angles from the ideal value of 90° for the ideal SP geometry to 98.2° in **3b**. A similar value has been reported for the $Ni^{(II)}$-dithioacetylacetonato, $[Ni(SacSac)_2]$, complex (97.2°).[50] Moreover, in order to reduce the ring strain and to accommodate the smaller bite, the P−N−P angles are contracted from 131.1° in ^{iPr,Ph}LK to 124.2° in **3b**. The Ph_2P−S bonds move toward the S−Ni−S plane (S−Ni−S−PPh_2 = 15.4°), giving rise to an overall ladder structure, in which the Ni−S−P−N−S−P are folded by 51.3° toward the ($^{i}Pr_2P$)S···P(Ph) direction.

Structural Preferences. Seven $Ni^{R,R'}L_2$ complexes have been structurally characterized up to now, namely $Ni^{Ph,Ph}L_2$ (**1*Td***),[9,24] **1SP**,[28] $Ni^{iPr,iPr}L_2$ (**2**),[25] $Ni^{Me,Me}L_2$,[23] $Ni^{nBu,tBu}L_2$,[26] $Ni^{Me,Ph}L_2$,[9] and $Ni^{iPr,Ph}L_2$ (**3**). The available crystallographic data show that when the ligands are symmetric (R = R′), the corresponding complexes display a distorted T_d geometry. Due to its high symmetry, the structure of **2** would serve as a reference structure among the family of $Ni^{R,R'}L_2$ complexes. In this structure, the N atoms are located in the S−Ni−S planes, while the P atoms are rotated out of it toward opposite sides, with the corresponding S−Ni−S−P torsion angles being exactly equal (15.4°). Therefore, the Ni−S−P−N−P−S metallacycle adopts a *twist* conformation, and the metal core of **2** displays an ideal S_4 point group symmetry, with the main axis bisecting both endocyclic S−Ni−S angles.[25] Furthermore, the endocyclic S−Ni−S angles are slightly less than 109.5° (see Supporting Information, Table S3), thus the core of **2** exhibits a minor tetragonal elongation, in contrast to what has been found for most T_d $[M(SAr)_4]^{2-}$ complexes (M = Fe,[15,51−55] Co,[15,16,51,52,55−59] Ni[12−18]) as well as the analogous $M^{iPr,iPr}L_2$ complexes (M = Mn,[33] Co,[60] Zn[25]), which are always compressed along the principal S_4 symmetry axis.

The T_d structure of **1*Td*** only approximates a compressed S_4 symmetry, since the Ni−S bond lengths and the S−Ni−S−P torsion angles are not exactly equal,[9,24] whereas the $Ni^{Me,Me}L_2$ complex exhibits a severely distorted T_d geometry, of an approximate C_{2v} symmetry.[23] On the other hand, when the ligands are asymmetric (R ≠ R′), the corresponding $Ni^{R,R'}L_2$ complexes display a SP geometry, with the Ni atom lying on a center of inversion. As mentioned above, $Ni^{Ph,Ph}L_2$ has been isolated in both geometries (**1*Td*** and **1SP**), being the only pair of NiS_4-containing stereoisomers reported up to date. It should be stressed, however, that the crystal of **1SP** contains also solvent molecules. The SP complexes **1SP** and **3** revert to their T_d paramagnetic isomers when they dissolve in common organic solvents, as confirmed by UV−vis, NMR, and magnetization studies, whereas complex **1SP** is transformed to **1*Td*** even in the solid state (vide infra). Only $Ni^{Me,Ph}$L keeps its SP diamagnetic geometry in solution.[9] The fact that $Ni^{Me,Me}L_2$ adopts a distorted T_d geometry[23] suggests that the repulsion between the R peripheral groups is not the dominant factor that promotes the T_d geometry.

The S−Ni−S endocyclic angles (see Supporting Information, Table S3), of all the $Ni^{R,R'}L_2$ complexes under investigation, can be compared with the ideal value of the T_d or SP geometry (109.5° and 90.0°, respectively). The deviation is only 1−3° for the T_d complexes, whereas it exceeds 8° for the SP complexes. This is not an unusual value for SP complexes containing six-membered chelating rings and has been ascribed to ring strain and potential repulsive interactions between the sulfur ligand atoms.[10,29] In contrast to the rest of the literature SP NiS_4 complexes,[9] which usually contain a rigid planar conjugated backbone and thus cannot tolerate very large bite angles, the structural flexibility of the dithioimidodiphosphinate ligands allows the corresponding SP $Ni^{R,R'}L_2$ complexes to revert to the less strained T_d geometry. Similar observations were made in the case of the SP and T_d isomers of the $Ni[^{i}Pr_2P(Se)NP(Se)^{i}Pr_2]_2$ complex.[32] We can, therefore, conclude that, although this family of ligands can accommodate both geometries upon coordination to $Ni^{(II)}$, the T_d geometry is more favorable, in contrast to what is common for Ni(II) complexes bearing different *S*,*S*′-chelating ligands, which usually exhibit SP geometry.[9]

Spectroscopic Studies. UV−vis Spectroscopy. The electronic spectrum of **3**, along with that of **1*Td***, in THF is shown in the Supporting Information, Figure S1. The spectrum of **3** shows a very intense CT band at 26 180 cm^{-1}

(50) Beckett, R.; Hoskins, B. F. *J. Chem. Soc., Dalton Trans.* **1974**, 622–625.
(51) Ueyama, N.; Okamura, T. A.; Nakamura, A. *J. Chem. Soc., Dalton Trans.* **1992**, 1019–1020.
(52) Okamura, T.; Takamizawa, S.; Ueyama, N.; Nakamura, A. *Inorg. Chem.* **1998**, *37*, 18–28.
(53) Coucouvanis, D.; Swenson, D.; Baenziger, N. C.; Holah, D. G.; Kostikas, A.; Simopoulos, A.; Petrouleas, V. *J. Am. Chem. Soc.* **1976**, *98*, 5721–5723.
(54) Coucouvanis, D.; Swenson, D.; Baenziger, N. C.; Murphy, C.; Holah, D. G.; Sfarnas, N.; Simopoulos, A.; Kostikas, A. *J. Am. Chem. Soc.* **1981**, *103*, 3350–3362.
(55) Huang, J.; Dewan, J. C.; Walters, M. A. *Inorg. Chim. Acta* **1995**, *228*, 199–206.
(56) Fukui, K.; Masuda, H.; Ohyanishiguchi, H.; Kamada, H. *Inorg. Chim. Acta* **1995**, *238*, 73–81.
(57) Otto, J.; Jolk, I.; Viland, T.; Wonnemann, R.; Krebs, B. *Inorg. Chim. Acta* **1999**, *285*, 262–268.
(58) Walters, M. A.; Dewan, J. C.; Min, C.; Pinto, S. *Inorg. Chem.* **1991**, *30*, 2656–2662.
(59) Chung, W. P.; Dewan, J. C.; Walters, M. A. *J. Am. Chem. Soc.* **1991**, *113*, 525–530.
(60) Gilby, L. M.; Piggott, B. *Polyhedron* **1999**, *18*, 1077–1082.

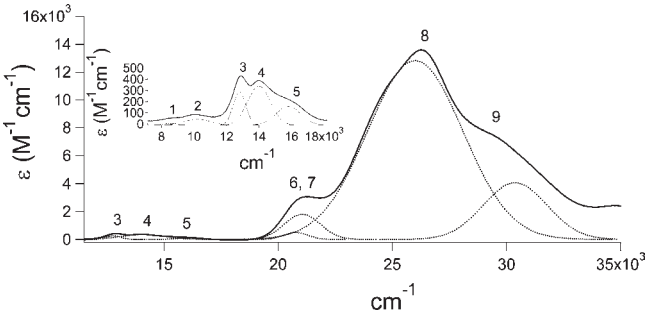

Figure 2. The UV−vis spectrum of complex **2** in CH_2Cl_2 fitted with Gaussian curves up to the "d−d" and CT transitions region. The inlet highlights the vis/NIR region of the spectrum.

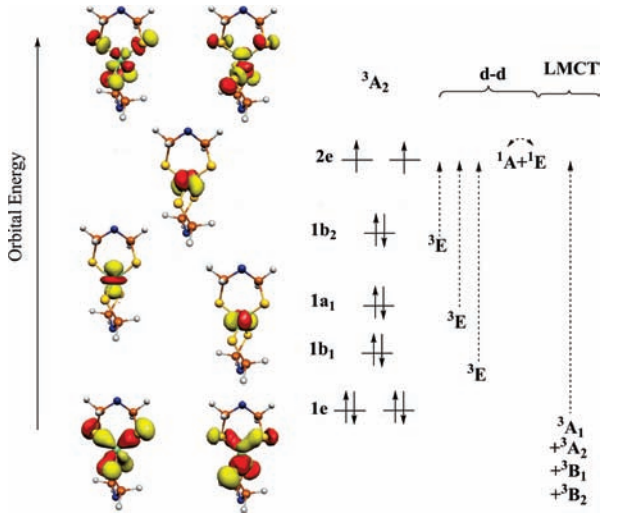

Figure 3. The metal−d-based MO and term symbols (analyzed under approximate D_{2d} symmetry), arising from single excitations in the elongated T_d $Ni^{H,H}L_2$ model. The indicated orbital occupation pattern refers to the $^3A_2$ ground state.

(ε = 5350 $M^{-1}cm^{-1}$) and that of $\mathbf{1}_{Td}$ at 25 870 cm^{-1} (ε = 7060 $M^{-1}cm^{-1}$), with a shoulder at 20 980 cm^{-1} (ε = 1010 $M^{-1}cm^{-1}$) and a low intensity feature which consists of two broad bands at 14 110 (ε = 154 $M^{-1}cm^{-1}$) and 12 760 cm^{-1} (ε = 175 $M^{-1}cm^{-1}$). The latter is assigned to the ν_3 $^3T_1(F) \rightarrow {}^3T_1(P)$ transition and is characteristic of T_d complexes with a distorted NiS_4 core.[27,61] The close resemblance of the two spectra suggests that, upon dissolution, complex **3** does not retain the SP geometry established in the solid state by X-ray diffraction, but it converts to a T_d $Ni^{II}S_4$ chromophore. This is further supported by ^{31}P NMR spectroscopy (vide infra). In Figure 2, a combined near IR−UV/vis absorption spectrum is presented for complex **2** in CH_2Cl_2. The Gaussian resolution obtained by simultaneous fitting of the spectrum gives rise to five distinguishable absorption bands for the lower-energy section of the spectrum, which reflects a distorted T_d $Ni^{(II)}S_4$ core. More specifically, the 1−6 bands correspond to transitions of "d−d" character, bearing in mind that the highest occupied−singly occupied molecular orbitals (HOMO−SOMO) involved are molecular orbitals with a significant ligand contribution, due to the covalent character of the Ni−S bonds (vide infra), as illustrated in Figure 3. In that respect, band 6 corresponds to a "d−d" transition, strongly overlapped by CT bands.[62] If we assume a T_d symmetry for the NiS_4 core, the low-energy band 2 (10 200 cm^{-1}, ε = 110 $M^{-1}cm^{-1}$) is assigned to the ν_2 $^3T_{1(F)} \rightarrow {}^3A_{2(F)}$ transition, whereas the bands 3−6 derive from transitions to the same excited term split by tetragonal elongation and spin−orbit coupling effects. This multicomponent band corresponds to the ν_3 ($^3T_{1(F)}$) → ($^3T_{1(P)}$) transition. By using the corresponding Tanabe−Sugano diagram, estimates of Δ_t = 5300 and B′ = 812 cm^{-1} are derived. Broadening of the peaks and distortion of the NiS_4 core to approximately D_{2d} symmetry leads to some uncertainty in assigning the center of the bands in terms of T_d symmetry. However, these values are consistent with those found for complex $\mathbf{1}_{Td}$.[27] Since the value of B for Ni^{2+}(g) ion is 1080 cm^{-1},[61] the nephelauxetic parameter β of complex **2** is approximately equal to 0.75, indicating a significant degree of covalency in the Ni−S bonds of such $Ni^{(II)}S_4$ systems. In the theoretical section, a full assignment of the bands, provided by multiconfiguration ab initio correlated methods, will be presented.

IR Spectroscopy. IR spectroscopy has been proved to be very helpful in investigating the effects exerted by the different peripheral R groups in $M^{R,R'}L_2$ complexes.[21] The IR spectrum of ^{iPr,Ph}LK is presented here for the first time (Supporting Information, Table S4). Deprotonation of the ^{iPr,Ph}LH ligand leads to the loss of the ν(N−H) band. The ν(P−N−P) band is shifted to higher frequencies, while the ν(P−S) bands are shifted to lower frequencies, compared to ^{iPr,Ph}LH,[36] in complete agreement with the shortening of the P−N bonds, the lengthening of the P−S bonds, and the overall enhancement of delocalization of π−electronic density upon deprotonation. A similar trend has been documented for the IR spectra of ^{Ph,Ph}LK,[21,48] ^{Me,Ph}LK[9] and for all the homoleptic $M^{R,R'}L_2$ complexes.[21] The above effects are manifested also in the IR spectrum of **3** (Supporting Information, Table S4). Moreover, it is noteworthy that the ν(P−N−P) bands of all the SP complexes are ∼50 cm^{-1} lower than the corresponding bands of the T_d complexes, a fact that is attributed not only to weaker P−N bonds but also to smaller P−N−P angles, since the "double-bond character" of the P−N−P fragment is decreased. This is corroborated by the crystal structures of the corresponding complexes, in which the P−N−P angles of the T_d species are significantly larger (by 10° or more) compared to the SP species (Supporting Information, Table S3). In that respect, the comparison between the $\mathbf{1}_{Td}$ (P−N−P = 130°) and $\mathbf{1}_{SP}$ complexes (P−N−P = 120°) is rather characteristic.

NMR Spectroscopy. The $^{31}P-\{^1H\}$ NMR spectrum of **3** (Supporting Information, Figure S3) shows two separate peaks, assigned to the two nonequivalent P atoms of the ligand, without any well-resolved hyperfine couplings. The NMR signals lie in the far paramagnetic region of the spectrum, supporting the conversion of **3** to a T_d NiS_4-containing site in solution, in agreement with the UV−vis data described above as well as the magnetic measurements (vide infra). It should be stressed that a similar SP → T_d isomerization takes place between $\mathbf{1}_{SP}$

(61) Figgis, B. N.; Hitchman, M. A. *Ligand Field Theory and Its Applications*; Wiley-VCH: New York, 2000.

(62) Nieto, I.; Bontchev, R. P.; Ozarowski, A.; Smirnov, D.; Krzystek, J.; Telser, J.; Smith, J. M. *Inorg. Chim. Acta* **2009**, *362*, 4449–4460.

Table 1. $^{31}P-\{^{1}H\}-NMR$ Spectroscopy Data of $^{R,R'}LK$ Ligands and $M^{R,R'}L_2$ Complexes[a]

compound	^{31}P chemical shifts (ppm)		
	Ph_2P	R_2P	^{2}J (P−P)
$^{Ph,Ph}LK$[48]	38.0	—	
$^{iPr,iPr}LK$ (this work)	—	60.8	
$^{iPr,Ph}LK$	36.8	72.4	13.1
$Co^{Ph,Ph}L_2$[60]	−32.8	—	
$Co^{iPr,iPr}L_2$[33,60]	—	−331.9	
$Co^{iPr,Ph}L_2$[33]	−87.8	−188.4	
T_d $Ni^{Ph,Ph}L_2$ (**1**$_{Td}$)[9,24]	−437.2	—	—
$Ni^{iPr,iPr}L_2$ (**2**)[25]	—	−725 (br)	
$Ni^{iPr,Ph}L_2$ (**3**)	−509.9	−553 (br)	
$Pd^{Ph,Ph}L_2$[63]	38.7	—	—
$Pd^{iPr,iPr}L_2$[64]		64.8	
$Pd^{iPr,Ph}L_2$[36]	37.1	69.3	12.8 Hz
$Pd^{PhO,PhO}L_2$[65]	45.1	—	—
$Pd^{PhO,Et}L_2$[36]	46.1	62.1	15.3 Hz
$Pd^{PhO,iPr}L_2$[36]	45.2	74.1	9.8 Hz

[a] Solvent: $CDCl_3$, 298 K.

and **1**$_{Td}$[28] as well as between the SP and T_d isomers of $Ni[^{i}Pr_2P(Se)NP(Se)^{i}Pr_2]_2$.[32] On the contrary, based on UV−vis and NMR data, the SP $Ni^{Me,Ph}L_2$ complex seems to retain its diamagnetic nature in solution.[9]

The ^{31}P chemical shifts of complexes **1**−**3** are collected in Table 1. From the comparison between the chemical shifts (Supporting Information, Figure S3), it becomes clear that in **3**, which contains the asymmetric $[^{i}Pr_2P(S)NP(S)Ph_2]^{-}$ ligand, the PPh_2 atom is shielded, whereas the $P^{i}Pr_2$ atom is deshielded, compared to the corresponding symmetric complexes **1**$_{Td}$ and **2**. For the analogous series of $Co^{R,R'}L_2$ complexes, we have already proposed the existence of an electron density flow from the P atom bearing the electron-donating ^{i}Pr groups to the P atom bearing the electron-withdrawing Ph groups, via the central metal atom.[33] The spectroscopic study of complexes **2** and **3** completes the $Ni^{R,R'}L_2$ series and further supports our proposal. The stronger paramagnetic shifts observed for the $Ni^{(II)}$ complexes (δ = −437 to −725 ppm) compared to the analogous $Co^{(II)}$ complexes (δ = −33 to −188 ppm)[33] is indicative of greater spin density on the ligands for the $Ni^{(II)}$ systems, consistent with the magnetic data analysis (vide infra).

We cannot make a similar comparison for the SP $Ni^{(II)}$ complexes, given the fact that **3** and **1**$_{SP}$ revert to their T_d paramagnetic isomers upon dissolution. However, a closer examination of the corresponding $Pd^{R,R'}L_2$ complexes,[36,63−66] which retain their SP geometry in solution, reveals that the P atoms bearing alkyl groups are deshielded, whereas the P atoms bearing the electron-withdrawing Ph or OPh groups are shielded, again compared to the corresponding symmetric complexes. Moreover, this trend is apparent in the ^{31}P NMR spectra of the potassium salts of the ligands (Table 1). Consequently, we can postulate that the aforementioned electron density flow is always present, regardless of the overall geometry. However, the diamagnetic nature of SP complexes limits this electron density flow.

The latter seems to play a substantial role in the stabilization of the boat conformation of the Ni−S−P−N−P−S chelating rings. In all the aforementioned complexes, the P atom that occupies one apex of the boat (hence the corresponding P−S bond is located out of the P−N−P and in the S−M−S plane) always "carries" Ph or other even stronger electron-withdrawing groups, like OPh and OEt. However, the stabilization of the boat conformation cannot be simply explained on the basis of different electron-donating or -withdrawing effects. In the crystal structure of $Pd^{EtO,Ph}L_2$, it is the Ph_2P-S bond that lies in the coordination plane (i.e., PPh_2 at the apex), although OEt is considered as a stronger electron-withdrawing group.[67] The tendency of the Ph_2P-S bonds to lie in the main coordination plane does not only stem from the electron-withdrawing properties of the Ph groups but also from their "in plane" orientation as well, which enhances the delocalization of electron density on this highly delocalized system.

Magnetic Properties of the SP Complexes. In order to study possible interconversions between the SP and T_d species, magnetic susceptibility measurements of the SP complexes **1**$_{SP}$ and **3** were conducted. Negligible evidence of any paramagnetic behavior has already been found for $Ni^{Me,Ph}L_2$, since it maintains its diamagnetic SP geometry both in the solid state and in solution.[9]

The results of the magnetic susceptibility measurements show that for complex **1**$_{SP}$, only 4.8% of the sample exists as a paramagnetic T_d compound at low temperatures (< 40 K). However, complex **1**$_{SP}$ reverts back to its T_d isomer (**1**$_{Td}$) at room temperature over time, indicating that the SP geometry is less stable than the T_d one. Measurement of the magnetic susceptibility for **3** reveals a similar, mainly diamagnetic signal with a small Curie tail, giving a 3% paramagnetic impurity. In contrast to **1**$_{SP}$, there is no rise of the magnetic susceptibility of **3** over time and temperature, implying that, in the solid state, **3** preserves its SP geometry. However, a paramagnetic nature of **3** is inferred in solution by UV−vis and NMR studies (vide supra). It can thus be concluded that the geometric preferences of **1**$_{SP}$, **3**, and $Ni^{Me,Ph}L_2$ are finely balanced. It appears that complex **1** prefers a SP geometry only at very low temperatures, with specific solvents of crystallization also being important.[28] Complex **3** is SP in the solid state even at room temperature, but it adopts a paramagnetic T_d geometry in solution. Finally, $Ni^{Me,Ph}L_2$ is the most stable SP complex among the three, since it preserves its geometry in solution.[9]

(63) Abbati, G. L.; Aragoni, M. C.; Devillanova, F. A.; Fabretti, A. C.; Garau, A.; Isaia, F.; Lippolis, V.; Verani, G. *J. Chem. Soc., Dalton Trans.* **2001**, 1105–1110.
(64) Cupertino, D.; Keyte, R.; Slawin, A. M. Z.; Woollins, J. D.; Williams, D. J. *Polyhedron* **1996**, *15*, 4441–4445.
(65) Nouaman, M.; Zak, Z.; Herrmann, E.; Navratil, O. *Z. Anorg. Allg. Chem.* **1993**, *619*, 1147–1153.
(66) Cupertino, D.; Birdsall, D. J.; Slawin, A. M. Z.; Woollins, J. D. *Inorg. Chim. Acta* **1999**, *290*, 1–7.
(67) Cupertino, D. C.; Keyte, R. W.; Slawin, A. M. Z.; Woollins, J. D. *Polyhedron* **1999**, *18*, 311–319.
(68) Figgis, B. N.; Lewis, J.; Mabbs, F. E.; Webb, G. A. *J. Chem. Soc. A* **1966**, 1411–1421.
(69) Boca, R. *Coord. Chem. Rev.* **2004**, *248*, 757–815.
(70) Boca, R. Structure and Bonding. *Magnetic Functions beyond the Spin−Hamiltonian*; Mingos, D. M. P., Ed.;Springer-Verlag: Heidelberg, Germany, 2006; Vol. *117*, pp 1−264.
(71) Maganas, D.; Kyritsis, P.; Groenen, E. J. J.; Neese, F. Manuscript in preparation.
(72) Fukui, K.; Kojima, N.; Ohyanishiguchi, H.; Hirota, N. *Inorg. Chem.* **1992**, *31*, 1338–1344.
(73) Vrajmasu, V. V.; Munck, E.; Bominaar, E. L. *Inorg. Chem.* **2004**, *43*, 4867–4879.

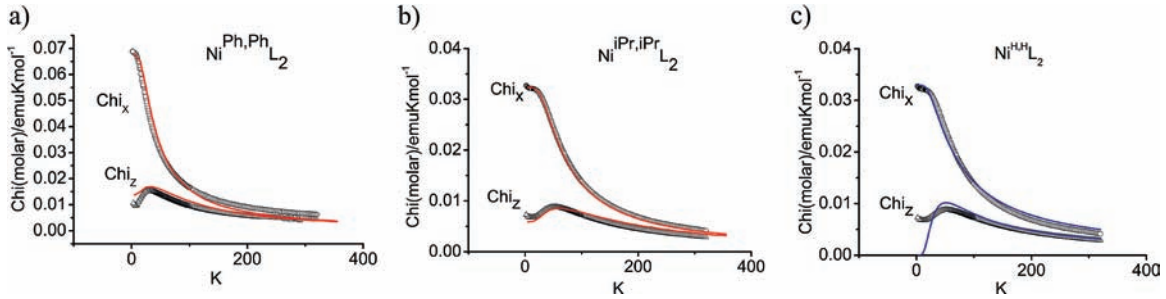

Figure 4. Magnetic susceptibility against temperature for (a) $\mathbf{1}_{Td}$ and (b) **2**, parallel and perpendicular to the unique axis. The red continuous lines were simulated using the procedure described by Figgis et al.[68] (c) The blue lines are fits to the experimental curves of complex **2,** with the close form of magnetic susceptibility equations, using the calculated $g_{\perp}$, $g_{//}$ and D parameters, as discussed in the Magnetic Properties Calculation Section (vide infra).

Table 2. Data Derived from the Analysis of the Magnetic Properties of Complexes $\mathbf{1}_{Td}$ and **2**

	axial field component, Δ (cm^{-1})	spin−orbit coupling constant, λ (cm^{-1})	orbital reduction factor, k
$\mathbf{1}_{Td}$	110	−45	0.5
2	200	−79	0.35

Magnetic Properties of the Td Complexes. The tetrahedral complex $\mathbf{1}_{Td}$ packs in a monoclinic unit cell that contains two independent molecules.[9,24] However, the *b* and *c* axes are almost equal and perpendicular to each other. Moreover, the molecules are oriented with the long molecular axis along the *a* direction. Thus, the two different molecules and the *b* and *c* axes have been regarded as equivalent, in order to simplify the magnetic analysis. The T_d complex **2** packs in a tetragonal unit cell, where the *a* and *b* axes are equivalent, and the *c* axis is unique. Variable-temperature magnetic susceptibility measurements were carried out on powder and single crystal samples of $\mathbf{1}_{Td}$ and **2**, with the applied magnetic field parallel and perpendicular to the unique *z* axis, which is defined as the N−Ni−N direction. Following the method described by Figgis et al.,[68] we applied the magnetic field perturbation (parallel and perpendicular to the unique axis) to the wave functions of the $^3T_1$ term, split by spin−orbit coupling and axial ligand field, and obtained the first- and second-order coefficients for substitution into the Van Vleck equation that describes the magnetic moment as a function of temperature. Due to the complexity of the resulting expression, we used trial values of the crystal field strength, the spin−orbit coupling constant (λ), the axial crystal field component (Δ), and the orbital reduction factor (k) to simulate the temperature-dependent susceptibility curves. The input parameters were altered by inspection, until an acceptable simulation of the experimental data was achieved (Figure 4a and b). A wide range of parameter combinations was investigated, and those reported are the only combinations that satisfactorily simulate the experimental data. Small discrepancies may be attributed to deviations from ideal axially distorted tetrahedral geometry in the crystal, which are larger for complex $\mathbf{1}_{Td}$[9,24] compared to **2**[25] as well as to imperfect alignment of the crystals parallel and perpendicular to the field direction. The resulting parameters derived for $\mathbf{1}_{Td}$ and **2** are given in Table 2. The data obtained for complex **2** are considered as more accurate, since its structural characteristics are closer to an axially distorted tetrahedral field, as required by the analysis employed by Figgis et al.[68] However, we believe that the data obtained for complex $\mathbf{1}_{Td}$, albeit less accurate, complement those obtained for **2**, reinforcing the conclusions drawn.

The cubic crystal field parameter was found to correspond to a weak field in both cases, as has been observed previously for T_d complexes which are typically weak field systems. This is also consistent with the UV−vis analysis (vide supra). The axial component of the crystal field was found to be relatively small for both complexes, and this is consistent with the small deviations from T_d geometry observed in the structural data. The most interesting parameters in this system are the orbital reduction factor (k) and the spin−orbit coupling constant (λ). The orbital reduction factor gives a measure of the spin density located on the metal center and varies between 1 and 0, corresponding to all the spin density located on the metal or all on the ligands, respectively. It should be noted that the values of k and λ should be considered together when interpreting physical properties of the complexes, as both parameters give an indication of spin density delocalization onto the ligands. Following the method by Figgis et al.,[68] k is introduced as a coefficient of λ when the Zeeman perturbation is applied, after the spin−orbit coupling perturbation. In interpreting the physical meaning of these two parameters, based on the low values of both, the conclusions described below are drawn but care is needed not to overinterpret the individual magnitude of each.

Simple inspection of the magnetic susceptibility curves for $\mathbf{1}_{Td}$ and **2** (Figure 4a and b) indicates that these complexes differ greatly from literature examples of T_d Ni$^{(II)}$ complexes,[68] since the peak in χ_z and the plateau in χ_x occur at much lower temperatures than is typical. The origin of this effect is revealed by the extremely low values of both k and λ for $\mathbf{1}_{Td}$ and **2** (Table 2).

In comparison, for a typical series of related complexes,[68] k takes values from 0.55 to 1.00, and λ varies between −130 to −224 cm^{-1}, with the free ion value at −315 cm^{-1}.[61] The very small orbital reduction factor gives a direct indication of the reduced spin density on the metal and, furthermore, the low value of the spin−orbit coupling constant arises from the same characteristic of the system. We are unaware of any prior examples where values of k and λ are both so low and interpret this unique behavior as arising from the noninnocent characteristics of the ligand, leading to a large amount of spin density located on the ligands.

In addition to the above parameters, for complex **2**, which exhibits an axially elongated S_4 geometry, it is meaningful to extract from our simulation the splitting between the $m_s = 0$ ground state and the lowest-lying $m_s = \pm 1$ excited states,[69,70] as described explicitly in the Supporting Information. This corresponds to the axial component, D, of the zero-field splitting (ZFS) employed in the spin Hamiltonian (SH) description of the $S = 1$ system (Supporting Information, Figure S2). A value of 77 cm^{-1} is estimated for complex **2**, which compares well with the calculated ZFS D values based on the theoretical calculations (vide infra). The analysis described above, comprising determination of the first- and second-order Van Vleck coefficients, considers the action of the spin and orbital components of the magnetic moment operator on the wave functions derived from the $^3T_1$ state. It is limited by the need to consider an axial system, whereas the SH approach, which does not explicitly consider orbital angular momentum, enables some rhombic character to be considered through the parameter E (vide infra). It is important to note that the resulting calculated value of E is negligibly small and that the values of D, determined by both approaches, are very similar. The consistency between the two approaches suggests that both are valid in providing a good description of the system.

Finally, in order to put the structural, magnetic, and electronic properties of complexes $\mathbf{1}_{Td}$ and **2** into perspective, we should make clear that they exhibit subtle structural differences, since they possess a tetragonally compressed and elongated NiS_4 core, respectively. This is expected to lead to different ground and excited states, as explicitly described when the effects of the *R* peripheral groups on the electronic properties of the system are taken into account (vide infra).

Quantum Chemical Calculations. Geometric Considerations. $Ni^{(II)}$ ($3d^8$) may form T_d, paramagnetic (high-spin, triplet, $S = 1$) or SP, diamagnetic (low-spin, singlet, $S = 0$) complexes, which exhibit very different properties. As discussed above, the T_d NiS_4 complexes display S_4 elongated or compressed structures. However, in the corresponding $Co^{R,R'}L_2$ complexes, it has been shown that the EPR properties, investigated by both experimental[34] and theoretical[71] methods, match those of $[Co(SAr)_4]^{2-}$ systems of D_{2d} symmetry.[72] In particular, using the annotation defined for the FeS_4-containing proteins rubredoxins, this structure approximates $D_{2d}(1)$,[73] being only lower due to ligand-constraining forces (i.e., the six-membered ring is not planar, torsion angle S−Ni−S−P > 0). Thus, for convenience we will adopt the symmetry labeling of the D_{2d} point group.

Interconversion Pathway between SP and T_d Geometries. Qualitative Discussion. It has been recognized that the reaction coordinate corresponding to the interconversion between the triplet T_d and the singlet SP states starts along a nuclear displacement that belongs to the representation E of the T_d symmetry point group. The two degenerate modes of E symmetry are shown in Scheme 1. Q_θ represents a nuclear motion which would result in compressing the ligands into the xy plane, while Q_ε is a twist, tending to put the ligands into the xz plane. Q_θ is defined by the δ_{S-Ni-S} angle along the S_4 principal axis (for an ideal T_d geometry $\delta_t = 109.5°$), while Q_ε is defined as the angle between the S−Ni−S/S−Ni−S planes α_1 (90°→0°) or the pairs of twisting exo−S−Ni−S angles α_2 (109.5°→180°).

Scheme 1[a]

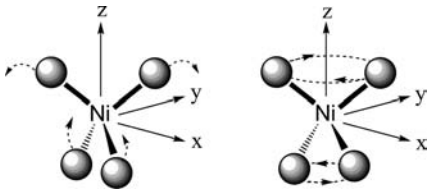

[a] The two *E*-symmetry bending modes Q_θ (left) and Q_ε (right), which dominate the Jahn−Teller (JT) distortion in T_d complexes.

Distortions along the two components of the E symmetry bending modes lead to two different SP conformations that are, in an idealized case, of D_{4h} and D_{2h} symmetry. For bidentate ligands, Q_θ cannot be operative because of ring strain. Therefore, it is mainly Q_ε that dominates the interconversion pathway. The $T_d \rightarrow$ SP interconversion pathway for complexes containing chelating ligands has been shown to follow the sequence $D_{2d} \rightarrow D_2 \rightarrow D_{2h}$.[74] For making comparisons easier, we will treat the isomerization procedure in the $Ni^{R,R'}L_2$ complexes by keeping the same symmetry notation.

In principle, there are two possible electronic configurations for a d^8 tetragonally distorted T_d system under the D_{2d} point group notation: (i) $[b_2^2e^2]$ for $\delta < \delta_t$, and (ii) $[b_2^1e^3]$ for $\delta > \delta_t$. These are related via two single electron excitations, namely $d_{xy} \rightarrow d_{xz}$ or $d_{xy} \rightarrow d_{yz}$ (Figure 3). The $D_{2d} \rightarrow D_{2h}$ isomerization proceeds via known routes, depending on the ground-state configuration of the D_{2d} structure and the number of Q modes that dominate.[74] If the twisting force along Q_ε is negligible, the value of δ will determine the ground-state configuration.[75] However, when both forces are active, the value of δ cannot provide a safe prediction of the triplet ground-state electron configuration.

The $T_d \rightarrow$ SP interconversion pathway in the $Ni^{R,R'}L_2$ complexes will be discussed in terms of: (i) spin−orbit coupling (SOC) in the ground state and (ii) Jahn−Teller (JT)-active excited states. The significant mixing of states provided by strong SOC interactions triggers and, in some cases, completely quenches the JT distortion forces.

Correlation between Ring Conformation and Geometry in the SP Complexes. The M−E−P−N−P−E metallacycles in transition-metal complexes of the general type $M[R'_2P(E)NP(E)R_2]_2$ (E = O, S, Se) can adopt different conformations (Supporting Information, Figure S4). Most of the T_d complexes of the first-row transition metals exhibit the same twist conformation, as the one observed in the crystal structure of complex **2** (vide supra). On the contrary, in all the SP complexes of $Ni^{(II)}$,[9,28] including complex **3**, and $Pd^{(II)}$[36,63−65] bearing the sulfido analogues, the metallacycles adopt the boat conformation (boat−SP) while, in the case of $Pt^{(II)}$,[19] the chair conformation (chair−SP). The twist conformation in a SP complex is only encountered in the $M[^iPr_2P(Se)NP(Se)^iPr_2]_2$ complexes, where M = Ni,[32] and Pt.[66]

(74) Lohr, L. L., Jr; Grimmelmann, E. K. *J. Am. Chem. Soc.* **1978**, *100*, 1100–1105.
(75) Mihail, A.; Cédrick, R.; Pio, B.; Claude, D. *Int. J. Quantum Chem.* **2005**, *102*, 119–131.

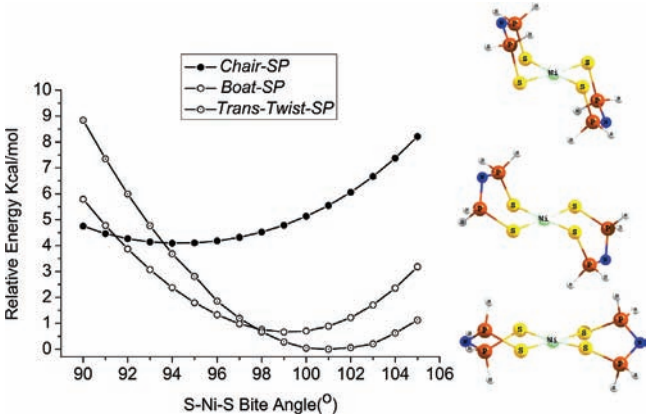

Figure 5. Correlation between the conformation of the Ni−S−P−N−P−S metallacycle and the S−Ni−S bite angle.

Since the P atoms that lie on the same side of the coordination plane are coordinated in a trans arrangement, we call this conformation trans−twist−SP. This results in an overall D_2 symmetry and corresponds to the D_{2h} structure of the $D_{2d} \rightarrow D_{2h}$ interconversion pathway, as found for the $Ni^{(II)}$ complexes containing chelating ligands, being only lower due to ligand-constraining forces.[74,76] We have performed relaxed potential scans along the S−Ni−S bite angle on the $Ni^{H,H}L_2$ model, keeping the α_2 angle constrained to 180°. From the diagram presented in Figure 5, it is evident that the chair−SP conformation can better accommodate smaller bite angles close to 90°, while, as the S−Ni−S angle opens up and the S···S distance increases, the boat−SP conformation is promoted. The cis−twist−SP conformation was considered as well but was found to be a transition state that relaxes back to the boat−SP conformation. It is concluded that, as the value of the bite angle increases, the chelating ring conformation changes from chair (∼90°) to boat (∼94°−98°) to twist (∼99°−104°). This is consistent with the experimentally observed trend. Factors that directly influence the E−M−E′ bite angle, such as the nature of the metal center (Ni, Pd, Pt) or the E donor atom (S, Se, Te),[32] would lead to different ground-state SP conformations.

Quantum Chemical Calculation of the Interconversion Pathway. It is well-known that the $T_d \rightarrow$ SP interconversion pathway is dominated by the strengthening of the ligand field (LF) as well as by orbital relaxation effects.[10,29] An additional insight into these phenomena can be provided by the theory of the pseudo-Jahn−Teller effect (PJTE).

Initially, we have constructed the DFT BP86/TZVP relaxed scanned potential energy surfaces for the triplet and singlet states, along the exo-S−Ni−S twisting angle α_2. The scan along $\alpha_2 > \alpha_t$ dominates the $D_{2d} \rightarrow D_2 \rightarrow C_i$ (A−C−D) interconversion pathway, while the scan along $\alpha_2 < \alpha_t$ dominates the $D_{2d} \rightarrow C_{2v}$ pathway, respectively, in agreement with previous findings.[10,29] In the particular case of $\alpha_2 > \alpha_t$, the MECP spin state occurs at $\alpha_2 = 140°$ (point C). This spin−crossover state lies only 3 kcal/mol higher than the T_d ground state, indicating a facile $T_d \rightarrow$ SP conversion. Overall six characteristic structures can be

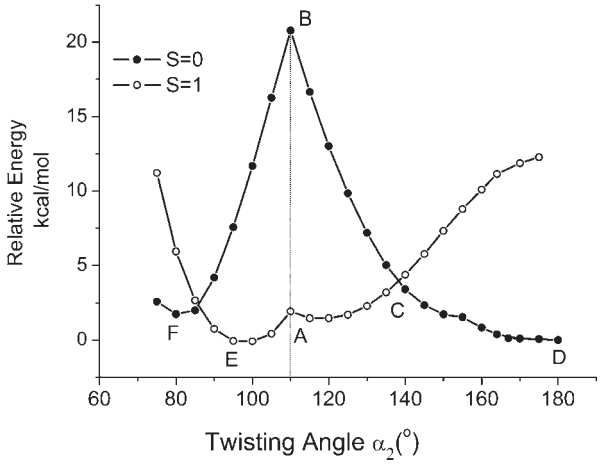

Figure 6. DFT BP86/TZVP constructed interconversion pathway along the α_2 exo-S−Ni−S twisting angle, by employing relaxed surface scans for the $S = 1$ and 0 states of $Ni^{H,H}L_2$ model complexes. The vertical line defines the $\alpha_2 > \alpha_{2t}$ (right) and $\alpha_2 < \alpha_{2t}$ (left) regions of the pathway.

identified along the interconversion pathway (points A−F; Figure 6 and Supporting Information Figure S4). A complete descriprion of the DFT-constructed pathway with respect to the structures identified along it is provided in the Supporting Information. It should be highlighted that, according to the DFT geometry optimizations, the $S = 1$ ground state is unstable around point A of Figure 6, which is contradictory to the experimental data. This inconsistency originates from a characteristic issue of DFT which, as a single determinant method, may fail to yield accurate electronic structures in which two or more configurations mix. Under D_{2d} symmetry, the two $^3A_2$ states (originating from $^3T_1$ in T_d symmetry) mix and reduce the JT stabilization energy (E_{JT}).[77] Despite this shortcoming, DFT methods are still useful to extract valuable information for the ground-state composition, along the interconversion pathway. Therefore, the ground-state electronic configuration observed at the starting point A of the interconversion pathway (Figure 6) is $b_2^2e^2$, which corresponds to an elongated T_d structure along the principal S_4 axis and is not JT in nature. However, the singly excited states of ^3E symmetry ($b_2^1e^3$) are subject to JT distortions, and they are expected to destabilize the ground state via PJTE.[78] In fact, by more carefully mapping the twist α_2 angle region from 90°−130° in steps of 1°, three well-distinguishable regions emerge (Figure 7a). From a Löwdin population analysis, it can be seen that in the $108° < \alpha_2 < 117°$ region, the $S = 1$ state corresponds to the $^3A_2(b_2^2e^2)$ electron configuration and displays approximate S_4 symmetry. Outside this region ($\alpha_2 < 107°$ or $\alpha_2 > 118°$), the dominant component of the triplet state originates from the $^3E(b_2^1e^3)$ configurations (corresponding to $d_{xy} \rightarrow d_{xz}$ and $d_{xy} \rightarrow d_{yz}$ excitations, respectively). It is concluded that, as the value of the δ angle deviates from δ_t, mixing of excited states that are JT-active destabilizes the ground state. Consequently, distorted T_d structures are observed, which are correlated with the $E \times e$ JTE of the $^3E(b_2^1e^3)$

(76) Starikov, A. G.; Minyaev, R. M.; Minkin, V. I. *Chem. Phys. Lett.* **2008**, *459*, 27–32.

(77) Reinen, D.; Atanasov, M.; Nikolov, G. S.; Steffens, F. *Inorg. Chem.* **1988**, *27*, 1678–1686.

(78) Garcia−Fernandez, P.; Bersuker, I. B.; Boggs, J. E. *J. Chem. Phys.* **2006**, *125*, article number: 104102.

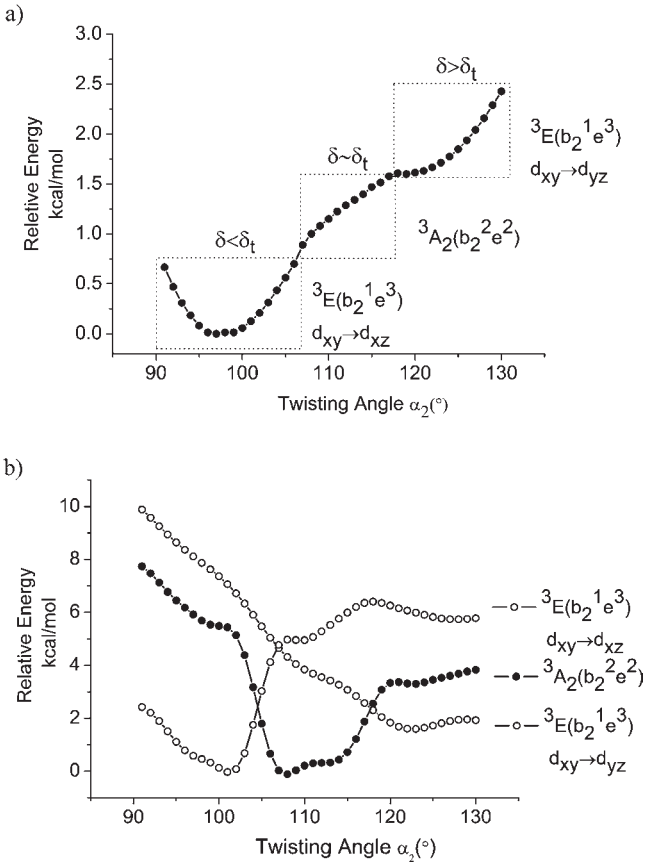

Figure 7. Identification of the twisting angle dependence of the $S = 1$ ground state, along the interconversion pathway derived from (a) DFT and (b) SACASCF(12,7) calculations.

state. We have so far treated the important spin-conserving excitations, which influence the ground state along the interconversion pathway. However, the $T_d \rightarrow$ SP isomerization of a d^8 transition-metal complex is a process that involves a transition between two states of different spin multiplicities. We, therefore, deal with two cooperative phenomena: a PJTE which involves spin-conserving excitations and a second procedure which involves spin-flipping excitations. Although such excitations are forbidden in high-spin, undistorted geometries, they might become allowed in distorted high-spin geometries due to enhanced molecular orbital mixing[78,79] that further stabilizes the low-spin configuration.

A more detailed approach can be provided via wave function-based multireference ab initio methods that treat the interacting states in a simultaneous and balanced way. State-averaged CASSCF(12,7) (SA-CASSCF) calculations were performed at the BP86 optimized structures (Figure 7b). Again, the energy of the three different electron configurations is plotted versus the twisting angle α_2. The failure of the DFT calculations to predict an energetic minimum for the $^3A_2$ ground state is alleviated in the SA-CASSCF calculations. A distinct local minimum is found for twisting angles between 107° and 117°, with the $^3A_2$-$(b_2^2e^2)$ configuration clearly dominating the ground state. On the other hand, the $^3E(b_2^1e^3)$ $(d_{xy} \rightarrow d_{xz})$ stabilizes for $\alpha_2 < 107°$ and dominates the ground state for $\alpha_2 < 103°$. The global stabilization minimum is at $\alpha_2 \sim 100°$ and corresponds to the $d_{xz}^2d_{xy}^1d_{yz}^1$ electron configuration. On the other hand, the $^3E(b_2^1e^3)$ $(d_{xy} \rightarrow d_{yz})$ state is stabilized for $\alpha_2 > 107°$ and dominates the ground spin state for $\alpha_2 > 117°$, showing a rather shallow minimum at $\alpha_2 \sim 120°$ $(d_{yz}^2d_{xy}^1d_{xz}^1$ electron configuration).

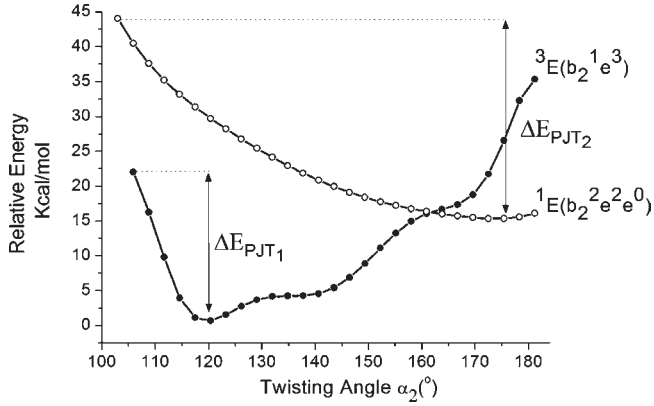

Figure 8. (a) Stabilization of the PJTE. MRDDCI2(7,12) energies of the $^3E(b_2^1e^3)$ and $^1E(b_2^2e^2e^0)$ states, respectively, inducing the spin crossover at the twisting angle $\alpha_2 = 161°$.

Dynamic Correlation Contributions. More accurate results can be obtained by including dynamic correlation contributions on top of the SA−CASSCF wave functions. To this end, MR−DDCI2(12,7) calculations have been performed (Figure 8). From these calculations, it is found that the triplet ^3E $(b_2^1e^3)$ JT-active excited state stabilizes for twisting angles $\alpha_2 > 119°$ compared to the $^3A_2(b_2^2e^2)$ ground state, in agreement with the SA-CASSCF calculations (Figure 7b). On the other hand, the singlet ^1E $(b_2^2e^2e^0)$ JT−active excited state dominates the ground state for $\alpha_2 > 161°$. It should be noted here that inclusion of dynamic correlation on top of the SA−CASSCF(12, 7) energies proved critical in order to predict such singlet triplet energetic crossings. The JT stabilization energy for the ^3E $(b_2^1e^3)$ $(d_{xy} \rightarrow d_{yz})$ triplet state is calculated to be $E_{PJT1} = 21.2$ kcal/mol at $\alpha_2 = 120°$ (Figure 8).

In agreement with previous findings,[74,77] under strong state-mixing conditions, the low-spin excited state of the undistorted geometry becomes the lowest in energy in the distorted configuration. Such distortion is accompanied by d orbital mixing, which lowers the symmetry of the charge distribution. However, as discussed above, a spin-flip excitation is necessary for the stabilization of the low-spin SP state, which can be thought as a $(^3A_2 + {}^1E) \times e$ PJTE distortion of the $b_2^2e^2e^0$ state, with $d_{xy}^2d_{xz}^2d_{yz}^0$ electron configuration. This phenomenon, i.e., that an overall ground-state structure originates from the distortion of a low-spin structure of higher energy than its high-spin counterpart, may be considered as a JT-induced spin crossover.[78,79] The MR-DDCI2 (12,7) JT stabilization energy for the ^1E singlet is $E_{PJT2} = 28.9$ kcal/mol ($\alpha_2 = 175.2°$). In fact, the ^1E state is stabilized in close agreement with the DFT results but sort of shifted (161° with respect to 145° in DFT) and dominates the $S = 0$ ground state for the twisting angles range of $\alpha_2 = 160°-180°$. Most important is the observation that the energy minimum of the ^1E state is larger by 17.1 kcal/mol compared to that of the corresponding $^3A_2$ state, and in accordance

(79) Bersuker, I. B. *Mol. Struct.* **2007**, *838*, 44–52.

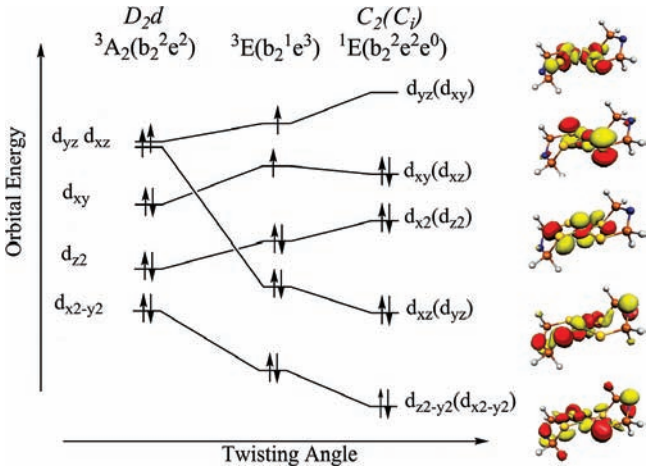

Figure 9. The MO diagram for the $D_{2d} \rightarrow C_2(C_i)$ isomerization of the $Ni^{R,R'}L_2$ complexes.

with the experimental data, it is not the preferred one for complexes with symmetric ligands. As it will be discussed in the next section, the stabilization of the SP $S = 0$ complexes involves stereochemical effects. However, the electronic origin of this is the induced symmetry lowering of the charge distribution of the $^3A_2(b_2^2e^2)$ and $^3E(b_2^1e^3)$ states in D_{2d} symmetry. The corresponding $d_{xy}^2d_{yz}^1d_{xz}^1$ and $d_{xy}^1d_{yz}^2d_{xz}^1$ or $d_{xy}^1d_{yz}^1d_{xz}^2$ configurations relax via the $D_{2d} \rightarrow D_2 \rightarrow C_i$ stabilization procedure to the $d_{xz}^2d_{xy}^1d_{yz}^1$ and $d_{xz}^2d_{xy}^2d_{yz}^0$ configuration (notation as for $z//N-Ni-N$ direction), respectively, stabilizing the ^1E ground spin state (Figures 8 and 9).

In summary, up to this point we have presented evidence, supported by X-ray crystallographic data and multiconfiguration ab initio calculations, that the interconversion pathway can be treated as a PJT-induced phenomenon (if the SOC or ligand field influence to the ^3E degenerate state are excluded). The results match the expected isomerization routes applied for elongated or compressed T_d $Ni^{(II)}$ complexes containing mono- and bidentate ligands.[75]

Spin−Orbit Coupling Contributions. Insight to the SOC contributions to the ground state as a function of the twisting angle α_2 is provided by the calculations of the SOC spin states presented in the Supporting Information, Figure S5. Although m_S is not a good quantum number, we will refer to the states as $|0\rangle$ and $|\pm1\rangle$, respectively. In accordance to the magnetic measurements on the D_{2d} limit of structural conformations (twisting angle range $108° < \alpha_2 < 117°$), the ground state, $^3A_2(b_2^2e^2, |0\rangle)$ is nonmagnetic. It is important to note that the minor stabilization energy of the ground spin state $^3E(b_2^1e^3, |\pm1\rangle)$ $(d_{xy} \rightarrow d_{yz})$ for larger twisting angles is accompanied with a strong SOC contribution from the low-lying states $^3A_2(b_2^2e^2, |0\rangle)$ and $^3A_2(b_2^2e^2, |\pm1\rangle)$ with $d_{xz}^1d_{xy}^2d_{yz}^1$ electron configuration. On the contrary, the SOC contribution is weaker to the corresponding $^3E(b_2^1e^3, |\pm1\rangle)$ $(d_{xy} \rightarrow d_{yz})$, leading to the strong stabilization of the $S = 1$ state for smaller twisting angles. It is, thus, evident that the SOC contribution via PJTE $(^3A_2 + {}^3E) \times e$ of the ^3E (high-spin) excited state mixing with the $^3A_2$ (high-spin) ground state largely affects the ground-state configuration, dominating the $D_{2d} \rightarrow D_2$ or the $D_{2d} \rightarrow C_{2v}$ pathways at large distorting angles, as discussed above. However, the net result of such strong state mixing is the quenching of the instability of the JT-active ^3E state by lifting its degeneracy, Supporting Information, Figure S5. The SOC even at around the highest symmetry point $\delta \sim \delta_t$ and $\alpha_2 \sim \alpha_t$ is sufficiently large to change the adiabatic potential energy surface (APES) morphology around it, from the JT "Mexican hat" APES to a parable with positive curvature (Figure 7b). We can, therefore, conclude that the ab initio treatment of the induced PJT interconversion pathway provides a complete description of the experimental structures observed, which otherwise would have led to incomplete structural explanations.

R Peripheral Group Effects. So far we have studied the electronic factors that promote the $D_{2d} \rightarrow D_2 \rightarrow C_i$ pathway. However, there are some drawbacks which do not allow the treatment of the problem as solely induced by JT phenomena. As discussed above, complexes with symmetric ligands will tend to be stabilized at the $S = 1$ D_{2d} structure, as is fact the case experimentally. In this section, the stereochemical factors that favor or oppose the action of the electronic factors will be included in the discussion of the observed X-ray structures. Symmetric $Ni^{R,R}L_2$ complexes will be stabilized along the inteconversion pathways, depending on their δ and α values. Complex **2** is the only elongated $M^{R,R'}L_2$ complex with zero twisting force, in agreement with the DFT calculations of the D_{2d} $Ni^{H,H}L_2$ model structure. We can, therefore, conclude that this structure is not PJTE influenced, and it can only exist in the minimum of the $b_2^2e^2$ configuration. On the other hand, compressed structures will be stabilized in the region of the $b_2^1e^3$ configurations, showing twisting distortions to an extent that will be controlled by the interactions between the peripheral R groups. In that respect, as Figure 7b shows, twisting distortions toward $\alpha < \alpha_t$ will stabilize the $S = 1$ state along the $D_{2d} \rightarrow C_{2v}$ pathway, as in the case of $Ni^{Me,Me}L_2$,[23] while twisting distortions to the opposite direction, $\alpha > \alpha_t$, will stabilize the $S = 1$ structures along the $D_{2d} \rightarrow D_2$ pathway, as in the case of $\mathbf{1}_{Td}$.[9,24] Due to the shallow D_2 minimum, under certain circumstances, both stereoisomers (T_d twist and SP trans−twist) can be observed, as in the case of $\mathbf{1}_{Td}$,[9,24] $\mathbf{1}_{SP}$,[28] and $Ni[^iPr_2P(Se)NP(Se)^iPr_2]_2$.[32]

On the other hand, in the presence of asymmetric ligands, strong deviations from the T_d geometry are expected due to the intrinsic structural characteristics of the ligands. This suggestion is supported by the structure of the asymmetric $^{iPr,Ph}LK$ ligand (vide supra), which upon its coordination to metal ions induces deviations from the T_d structure, as in the case of the $M^{iPr,Ph}L_2$ (M = Mn, Co) complexes.[33] For the Ni(II) complexes involving asymmetric ligands, the singlet excitation $b_2^2e^1e^1 \rightarrow b_2^2e^2e^0$ via spin-relaxation effects (depicted in Figure 9) becomes allowed, and therefore, the SP $S = 0$ geometry might be stabilized, as in the case of the $Ni^{Me,Ph}L_2$[9] and **3** complexes.

Spin Density Delocalization and Covalency. The calculated electron and spin populations at the BP86 level for the triplet and singlet ground states in D_{2d} and $SP(C_i)$ geometries reflect a strongly covalent NiS_4 site, with significant differences observed between the two cases. The bonding in the D_{2d} case is 'traditional' with the metal d−orbitals being at higher energy than the ligand orbitals. In the $SP(C_i)$ case, an 'inverted bonding' description is

Table 3. The Calculated d−d and LMCT Triplet−Triplet Vertical Excitation Energies of Complex **2**[a]

ground state	state (transition)	DDCI2(12,7)		SORCI(12,7)		expt
$^3A_2\rightarrow$	$^3E(1b_2 \rightarrow 2e)$	3019		3157		−
		3027		3201		−
	$^3E(1a_1 \rightarrow 2e)$	4567		5043		−
		4569		5196		−
	$^3B\ (1b_1 1b_2 \rightarrow 2e)$	9371	9439	8719	8719	8500
			9439		8720	
			9719		8991	
	$^3A_2(1b_1, 1a_1 \rightarrow 2e)$	11 094	11 415	10558	10 879	10 200
			11 549		11 003	
			11 550		11 004	
	spinflip	12 127	12 127	12 242	12 242	∼12 800−16 100
		13 039	13 039	12 377	12 377	
		15 817	15 817	15 141	15 141	
		16 263	16 263	16 004	16 004	
		16 267	16 267	16 125	16 125	
	$^3E(1b_1 \rightarrow 2e)$	17 042	17 103	17 022	17 070	
			17 122		17 090	
			17 569		17 364	
		17 066	17 586	17 070	17 396	
			17 590		17 502	
			17 825		17 659	
	$^3A_2(1a_1 1b_2 \rightarrow 2e)$	20 893	21 203	19 272	19 546	∼20 500[b]
			21 203		19 546	
			21 241		19 578	
	LMCT(1e → 2e)	25 134−26 476		28 850−29 468		∼21 000−29 000

[a] In cm^{-1}, relative to the lowest $^3A_2$ state. Their assignment is based on MR-DDCI2 and SORCI calculations. For the experimentally important d−d transitions, the SOC corrected energies are also presented (second subcolumn). The calculations were performed on a model structure of $Ni^{iPr,iPr}L_2$ in which the ^{i}Pr peripheral groups were replaced by H and were optimized at the BP86 level for their positions. [b] The transition $^3A_2(^3T_1, F) \rightarrow {}^3A_2(^3T_1, P)$ likely overlaps with LMCT and or ligand-based transitions.

obtained in which the ligand orbitals are situated at higher energy than the metal d orbitals. This behavior has been reported previously for Ni bis(dithiolene) SP complexes.[80]

The Löwdin population analysis from the BP86 calculations provide 1.5 unpaired electrons on the Ni center and 0.5 unpaired electrons on the sulfur ligands, indicating significant S → Ni charge donation. This can also be seen in the quasirestricted molecular orbital diagram in Figure 3. The d_{yz} and d_{xz} MOs will be involved in covalent interactions with the corresponding S lone pair (LP) orbitals, providing σ-covalent Ni−S bonding interactions. In addition, a more complete picture is revealed from the localized β spin S LPs which are distributed in the Ni−S−P sequence as 25% Ni, 70% S, and 5% P. Thus, this data indicates significant spin delocalization from the metal to the ligand via a π-pathway. This trend is also reflected in the values of the P−N−P angles of the T_d and SP $Ni^{R,R'}L_2$ complexes (Supporting Information, Table S3) and supported by experimental data, such as the ^{31}P NMR paramagnetic shifts (Table 1) as well as the orbital reduction factor k (Table 2) determined by the analysis of magnetic properties (vide supra). In the SP $Ni^{H,H}L_2$ model, the decrease of the S−Ni−S bite angle to 98° results in better alignment of the S−3p orbitals with respect to the Ni−$3d_{xy}$ orbital, increasing their mixing, as reflected in the Löwdin population analysis of the Ni d_{xy}−S 3p (50.4 and 49.6%, respectively), thus showing a stronger Ni−S σ-bond relative to the T_d isomers. In fact, the lowest unoccupied molecular orbital (LUMO) is the antibonding combination of the Ni−$3d_{xy}$ and the ligand σ in-plane−out-of-phase orbitals. Due to the ligand geometry, the overlap between these two orbitals is highly favorable, providing an efficient pathway for ligand-to-metal charge donation and thus resulting in a highly covalent Ni−S bond.

Excited States. In this section, a full interpretation of the absorption spectrum of complex **2** is performed by MR-DDCI2 and SORCI dynamic correlated methods, taking into account the SOC interactions. The calculations confirm the experimental observations, predicting that the bands in the visible region of the spectrum, shown in Figure 2 and Table 3, are composed from $^3A_2 \rightarrow {}^3B(1b_2, 1a_1 \rightarrow 2e, {}^3F)$, $^3A_2 \rightarrow {}^3A_2(1b_1 1b_2 \rightarrow 2e, {}^3F)$, $^3A_2 \rightarrow {}^3E(1b_1 \rightarrow 2e, {}^3P)$, and $^3A_2 \rightarrow {}^3A_2(1a_1 1b_2 \rightarrow 2e, {}^3P)$ "d−d" excitations, respectively. As discussed in the Experimental Section, the room-temperature experimental spectra of $\mathbf{1}_{Td}$ and **2** reveal multicomponent bands being traditionally assigned as $^3A_2 \rightarrow {}^3T_1(^3P)$ excitations, that are split by low-symmetry and SOC effects.[61] Spin-forbidden transitions are calculated very close to the $^3A_2 \rightarrow {}^3E$ $(1b_1 \rightarrow 2e, {}^3P)$ transitions, thus they might gain intensity and contribute to the shape of the multicomponent band. In fact, an average of a non-negligible borrowing intensity with an oscillator strength 6.0×10^3 is calculated for these spin-forbidden transitions.

The $^3A_2 \rightarrow {}^3A_2$ $(1a_1 1b_2 \rightarrow 2e, {}^3P)$ excitation is predicted at ∼19 000 cm^{-1}, with very low intensity. In the experimental spectrum, it is presumably obscured by CT excitations, as can be seen in the Gaussian resolution analysis in Figure 2. In the CT region, the first three LMCT triplet−triplet vertical excitations originate to the 1e → 2e electron promotions (Figure 3). The most intense band with an oscillator strength of 2.1×10^6 is calculated at 28 850 cm^{-1}, in very good agreement with the experimental spectrum.

Magnetic Properties Calculation. The 45 microstates that span the d^8 ligand field manifold will split under the action of the low-symmetry crystal field and the SOC. The SOC states can be classified according to double

(80) Szilagyi, R. K.; Lim, B. S.; Glaser, T.; Holm, R. H.; Hedman, B.; Hodgson, K. O.; Solomon, E. I. *J. Am. Chem. Soc.* **2003**, *125*, 9158–9169.

group symmetry, as shown in the Supporting Information, Figure S2. In the case of tetragonally elongated structures, the ZFS has its usual meaning, and one obtains large and positive D values ($\varepsilon\Gamma_5 - \varepsilon\Gamma_1$), consistent with the nonmagnetic behavior observed experimentally. Although the m_S is not a good quantum number, we will refer to the states as $|0\rangle$ and $|\pm1\rangle$, respectively.

Attempts to experimentally observe EPR signals of the $S = 1$ T_d $Ni^{R,R'}L_2$ complexes proved unsuccessful. Complex $\mathbf{1}_{Td}$ remained EPR silent up to extremely high-magnetic fields (15 T) and frequencies (600 GHz).[81] Therefore, the ZFS in this system is expected to exceed 25 cm^{-1}. In the following, we provide a systematic interpretation of the SH parameters of such systems from the point of view of quantum chemical calculations. The findings are compared with the experimental magnetic measurements discussed above.

Spin Hamiltonian Parameters: g tensor, ZFS. In order to interpret the **g** and **D** tensors of the D_{2d} elongated NiS_4 core, it is important to know the selection rules of the SOC operator. Under D_{2d} symmetry, the z component transforms as B and the x,y components as E. Thus, the ^{3}B state has nonzero SOC with B states via the z component as well as with E states via the x,y components. The **g** tensor calculated by the B3LYP method shows, as expected, small deviations from the free-electron value along the S_4 axis, which coincides with the N−Ni−N direction ($g_{||} = 2.0031$) and significantly large values perpendicular to it ($g_\perp = 2.367$). These results suggest that the large positive $\Delta g_\perp$ is dominated by contributions from the $^3E(1b_2 \rightarrow 2e)$ state and much less by contributions from $^3E(1b_1 \rightarrow 2e)$ because the former represents a transition from a doubly to a singly occupied orbital, which is associated with positive **g** shifts.[82,83]

Quantitative predictions of the ZFS tensor to a first approximation were performed with the recently proposed linear response DFT theory.[71] The B3LYP/TZVP coupled−perturbed CP method is used for the calculation of the ZFS values, which uses revised prefactors for the spin−flip terms and solves a set of coupled−perturbed equations for the SOC perturbation, as described elsewhere in details.[84] The D^{ss} part accounting for the spin−spin interactions to the ZFS is treated with the 'UNO' option which allows the calculation of the SS term with a restricted spin density obtained from the singly occupied unrestricted natural orbitals. By employing the above method, we arrive to the following ZFS values: $D = +58$ cm^{-1} and $E/D = 0$. The origin of the ZFS arises particularly from spin−orbit coupling ($D^{soc} = 56$ cm^{-1}), originating from spin-conserving excitations to the SOMOs $^3E(2b_1 \rightarrow 2e)$, $^3E(1a \rightarrow 2e)$, and $^3E(1b_2 \rightarrow 2e)$, while only 3% involves spin−flip forbidden excitations. The spin−spin interactions account only for ~4% (3 cm^{-1}) of the D value. Thus, these results are surprisingly good, given that in the presence of near orbital degeneracy, all quantum chemical methods have difficulties to predict accurate values of the SH parameters.

In general, multiconfigurational ab initio calculations are more suitable in the presence of near orbital degeneracy than in DFT methods because they can represent all magnetic sublevels explicitly and on an equal footing. Thus, the combination with the quasidegenerate perturbation theory is suitable to attack problems of the kind met here. In the QDPT approach, the SOC (and SS) effects are treated through diagonalization of the SOC (and SS) operators, in the basis of the triplet and singlet roots obtained from SA-CASSCF or MR-DDCI or SORCI calculations.

Anisotropic covalency is introduced at the level of the molecular orbitals, from which the multiconfigurational states are constructed. Unfortunately, Hartree−Fock-based methods, such as CASSCF, will strongly underestimate metal−ligand mixing and, hence, underestimate anisotropic covalency. This shortcoming is very important since the estimated covalency from magnetic measurements is large ($k \sim 0.35-0.5$). However, in correlated ab initio MR-DDCI or SORCI calculations employed on top of the CASSCF wave functions, these shortcomings are considerably reduced and, therefore, realistic predictions of the ZFS are expected. In addition to the second-order perturbation theory equations for the ZFS, ab initio methods treat the triplet and singlet states in infinitive order. We can, therefore, extract the ZFS parameter D by using the exact solution of the $S = 1$ SH problem for the ZFS. In fact, for the axially elongated structure at twisting angle $\alpha_2 = 110$, the MR-DDCI calculation up to the second-order perturbation theory predicts a value of $D = 73$ cm^{-1} ($E/D = 0.07$). Furthermore, calculation of the eigenvalues of the diagonalized 3×3 ZFS matrix gives the energy separation between the two ground spin states as $D = (\varepsilon\Gamma_5 - \varepsilon\Gamma_1) = 60$ cm^{-1}.

We have furthermore checked the consistency of the DFT prediction method with well established semiquantitative ligand field methods, by employing standard ligand field arguments combined with excited state energies calculated by correlated ab initio methods.[82] The computations indicate that there are major contributions from excitations, which occur within the triplet state. The final value of $D = 55$ cm^{-1} is fairly realistic for tetrahedraly coordinated d^8 high-spin complexes and is consistent with the DFT and the multireference ab initio calculated values of $D = 57$ and 60 cm^{-1}, respectively. In an effort to check the reliability of the calculated ZFS as well as the $\mathbf{g}_z$ and $\mathbf{g}_{xy}$ values, we performed a reconstruction of the experimental magnetic susceptibility components by using the closed form formulas for the susceptibility components of an axial ZFS system[69,70] ($S = 1$, $E = 0$). Analytical expressions of the equations are provided in the Supporting Information. The fitting to the experimental data for $Ni^{iPr,iPr}L_2$ is fairly satisfactory (Figure 4c).

Conclusions

In this work, the synthesis and thorough characterization of a NiS_4-containing complex, $Ni^{iPr,Ph}L_2$ (**3**), bearing the asymmetric dithioimidodiphosphinate $^{iPr,Ph}L^-$ ligand, is described. Complex **3** completes the series of Ni(II) complexes involving the respective symmetric ligands, namely $Ni^{Ph,Ph}L_2$ (**1**) and $Ni^{iPr,iPr}L_2$ (**2**). The nature of the R peripheral group

(81) Krzystek, J.; Ferentinos, E.; Maganas, D.; Kyritsis, P. Unpublished results.
(82) Neese, F.; Solomon, E. I. *Magnetoscience − From Molecules to Materials*; Miller, J. S., Drillon, M. Ed.; **2003**; Vol. *IV*, p 345.
(83) Neese, F.; Solomon, E. I. *J. Am. Chem. Soc.* **1998**, *120*, 12829–12848.
(84) Neese, F. *J. Chem. Phys.* **2007**, *127*, article number: 164112.

(Ph or ^{i}Pr) in defining the NiS_4 core geometry and, consequently, the corresponding ground spin state, were shown to be crucial. Crystallographic data and spectroscopic studies in the solid state and in solution have proved that the SP NiS_4 geometry is observed under specific conditions, only in the solid state (complexes $\mathbf{1_{SP}}$ and **3**), whereas in solution there is clear preference for the T_d geometry of all three, **1**−**3**, complexes. The above observations are confirmed by theoretical calculations which show that a symmetric $^{R,R}L^-$ ligand environment would tend to stabilize a T_d NiS_4 structure as well as the $S = 1$, $^3A_2(b_2^2e^2)$, ground spin state, against the expectations stemming from ligand field theory arguments. This state, however, might be unstable due to the contribution of the $^3E(b_2^1e^3)$ JT-active excited states, which induce a strong orbital mixing and initiate the $T_d \rightarrow$ SP interconversion pathway, in terms of a $D_{2d} \rightarrow D_2 \rightarrow C_i$ symmetric sequence. Such orbital mixing can be enhanced in complexes with asymmetric $^{R,R'}L^-$ ligand environments, thus leading to a SP NiS_4-core geometry and a singlet ground state, as has been experimentally observed for $Ni^{Me,Ph}L_2$ and complex **3**.

In addition, detailed SQUID measurements on oriented crystals of complexes **1** and **2** are consistent with extensive delocalization of spin density toward the ligands, a finding with wider implications concerning the nature of Ni−S bonds in nickel enzymes,[3−5] despite the nonbiological nature of the dithioimidodiphosphinate ligands. Along these lines, previous investigations on the covalency of Ni−S bonds have employed sulfur K-edge X-ray spectroscopic studies on both T_d and SP NiS_4- and NiS_2N_2-containing complexes, respectively, but in this case, the ligands employed were of different types.[85,86] The findings of our work, combined with earlier investigations,[9,28,32] confirm that dichalcogenated (S or Se) imidodiphosphinate types of ligands can afford either T_d or SP complexes based either on different R peripheral groups or, simply, on different experimental conditions. The versatile coordinating properties of the ligands employed in this work toward $Ni^{(II)}$ are evident, since the analogous NiS_4 complexes containing six-membered Ni−S−P−N−C−S chelating rings have so far been shown to be exclusively SP.[87−92]

Of special importance is the experimental and theoretical evidence, presented herein, for a strong spin−orbit coupling in the paramagnetic T_d NiS_4 complexes studied, leading to large ZFS values, which will be a challenge to confirm by appropriate experimental methods as EPR,[34,93,94] MCD,[93] and Far-IR magnetic spectroscopy.[95]

Collectively, our work can form the basis of investigating structure−properties relationships in other NiS_4-containing systems.

Acknowledgment. We thank the University of Edinburgh, School of Chemistry crystallography service for data collection and structure solution of complex **3** and Frank Mabbs, University of Manchester for useful discussions on the magnetic simulation. D.M. and F.N. acknowledge financial support from the DFG priority program SFB 813 "Chemistry at Spin Centers". P.K. thanks the Special Account of the University of Athens (grant 7575) and the Empirikion Foundation for funding as well as Prof. Georgios Pneumatikakis for his support. The referees of the manuscript are thanked for their constructive comments.

Supporting Information Available: Table S1, crystallographic data for $^{iPr,Ph}LK$ and complex **3**; Table S2, selected bond lengths and angles of $^{iPr,Ph}LH$, $^{iPr,Ph}LK$, and **3b**; Table S3 a and b selected bond lengths and angles of SP and T_d $Ni^{R,R'}L_2$ complexes; Table S4, IR data; Figure S1, electronic spectra of $\mathbf{1}_{Td}$ and **3**; Figure S2, energy level diagram for four-coordinate high-spin Ni(II) complexes, and relevant analysis; Figure S3, $^{31}P-\{^1H\}$ NMR spectra; Figure S4, the most important $Ni^{H,H}L_2$ structures, and relevant analysis; Figure S5, the $^3A_2(b_2^2e^2)$ and $^3E(b_2^1e^3)$ SOC spin states as well as the LF−ZFS model equations and magnetic susceptibility equations. This information is available free of charge via the Internet at http://pubs.acs.org.

(85) Williams, K. R.; Hedman, B.; Hodgson, K. O.; Solomon, E. I. *Inorg. Chim. Acta* **1997**, *263*, 315–321.
(86) Szilagyi, R. K.; Bryngelson, P. A.; Maroney, M. J.; Hedman, B.; Hodgson, K. O.; Solomon, E. I. J. *Am. Chem. Soc.* **2004**, *126*, 3018–3019.
(87) Iwamoto, T.; Ebina, F.; Nakazawa, H.; Nakatsuka, C. *Bull. Chem. Soc. Jpn.* **1979**, *52*, 1857–1858.
(88) Zak, Z.; Glowiak, T.; Chau, N. T. T.; Herrmann, E. *Z. Anorg. Allg. Chem.* **1990**, *586*, 136–140.
(89) Sokolov, F. D.; Zabirov, N. G.; Brusko, V. V.; Krivolapov, D. B.; Litvinov, I. A. *Mendeleev Commun.* **2003**, 72–73.
(90) Brusko, V. V.; Rakhmatullin, A. I.; Shtyrlin, V. G.; Krivolapov, D. B.; Litvinov, I. A.; Zabirov, N. G. *Polyhedron* **2006**, *25*, 1433–1440.
(91) Safin, D. A.; Sokolov, F. D.; Gimadiev, T. R.; Brusko, V. V.; Babashkina, M. G.; Chubukaeva, D. R.; Krivolapov, D. B.; Litvinov, I. A. *Z. Anorg. Allg. Chem.* **2008**, *634*, 967–971.
(92) Safin, D. A.; Sokolov, F. D.; Szyrwiel, Ł.; Babashkina, M. G.; Gimadiev, T. R.; Hahn, F. E.; Kozlowski, H.; Krivolapov, D. B.; Litvinov, I. A. *Polyhedron* **2008**, *27*, 2271–2276.
(93) Krzystek, J.; Zvyagin, S. A.; Ozarowski, A.; Fiedler, A. T.; Brunold, T. C.; Telser, J. *J. Am. Chem. Soc.* **2004**, *126*, 2148–2155.
(94) Krzystek, J.; Swenson, D. C.; Zvyagin, S. A.; Smirnov, D.; Ozarowski, A.; T., C.; Telser, J. *J. Am. Chem. Soc.* **2010**, *132*, 5241–5253.
(95) Vongtragool, S.; Gorshunov, B.; Dressel, M.; Krzystek, J.; Eichhorn, D. M.; Telser, J. *Inorg. Chem.* **2003**, *42*, 1788–1790.